### Title
Microdystrophins partially rescue deficits of Duchenne muscular dystrophy iPSC-cardiomyocytes




### Journal
Molecular Therapy Advances, 34(3)

### ISSN
3117-387X



### Authors
Keegan, Abiageal R
Gonzalez, Adriana Fernanda GS
Zhang, Rongruo
et al.



### Publication Date
2026-09-01

### DOI
10.1016/j.omta.2026.201801

Molecular Therapy
Advances
Original Article

# Microdystrophins partially rescue deficits of Duchenne muscular dystrophy iPSC-cardiomyocytes

Abiageal R. Keegan,[1,3,4] Adriana Fernanda G.S. Gonzalez,[2] Rongruo Zhang,[2] Hung Doan,[2] Sofía I. Torres-Bigio,[2] Fiona Lau,[2] Kaulen N. Ly,[2] Elaine C. Lai,[2,3,4] Leahlyn C. Mamuyac,[2] Sriram Bhimaraju,[2] Abhishree Mishra,[2] Michelle K. Polen,[2,3,4] Daniel S. Ortiz,[3,5] Jay H. Lam,[3] and Asuka Eguchi[2,3,4,6,7]

[1]Mathematical, Computational, and Systems Biology Graduate Program, University of California, Irvine, Irvine, CA 92697, USA; [2]Department of Physiology and Biophysics, University of California, Irvine, Irvine, CA 92697, USA; [3]Sue and Bill Gross Stem Cell Research Center, University of California, Irvine, Irvine, CA 92697, USA; [4]Muscle Biology and Disease Research Center, University of California, Irvine, Irvine, CA 92697, USA; [5]Department of Molecular Biology and Biochemistry, University of California, Irvine, Irvine, CA 92697, USA; [6]Edwards Lifesciences Foundation Cardiovascular Innovation and Research Center, University of California, Irvine, Irvine, CA 92697, USA; [7]Department of Biomedical Engineering, University of California, Irvine, Irvine, CA 92697, USA

**Duchenne muscular dystrophy (DMD) is a severe muscle wasting disease caused by the lack of dystrophin. Dilated cardiomyopathy is the leading cause of death in DMD patients. Smaller variants of dystrophin, called microdystrophins, amenable to packaging into adeno-associated virus (AAV), have been shown to be effective in improving skeletal muscle function in animal models. However, the functional benefit of these microdystrophins in the DMD heart remains unclear. To determine the efficacy of microdystrophin gene therapy, we compared three microdystrophin variants in DMD cardiomyocytes (CMs) differentiated from human induced pluripotent stem cells (iPSCs). We used three DMD lines of different genetic backgrounds and benchmarked against controls expressing full-length dystrophin. We also tested a dystrophin variant, minidystrophin, which is larger than the microdystrophins. Our results show that microdystrophins partially rescue disease phenotypes; however, the results are variable among genetic backgrounds. Global transcriptional profiling revealed that gene therapy altered the disease signatures of DMD iPSC-CMs. Minidystrophin significantly improved cell viability of DMD CMs in two of three lines of different genetic backgrounds. Minidystrophin also reduced arrhythmic events in one genetic background. Our findings suggest that the delivery of larger dystrophin variants may be more beneficial to delaying the onset of cardiac complications.**

## INTRODUCTION

Duchenne muscular dystrophy (DMD) is a progressive, muscle-wasting genetic disorder that affects nearly 1 in every 5,000 live male births.[1] DMD patients suffer from muscle weakness that ultimately leads to a loss of ambulation in their teens, and the leading cause of death in these patients is heart failure.[2] By contrast, Becker muscular dystrophy (BMD) progresses more slowly than DMD, and like DMD patients, most BMD patients develop cardiomyopathy.[3,4] DMD is caused by the lack of dystrophin expression, whereas BMD involves the expression of a truncated dystrophin often at lower levels.[5] Dystrophin stabilizes the sarcolemma of muscle cells by transducing force from the cytoskeleton to the extracellular matrix.[6,7] The dystrophin protein comprises the N terminus, the central rod domain, the cysteine-rich domain, and the C terminus.[8] The N terminus serves to bind actin filaments, and the deletion of this domain is associated with early onset cardiomyopathy.[9,10] The central rod domain functions to transduce force from the inside to the outside of the cells.[11] The cysteine-rich region binds to the dystroglycan complex, which enables bridging of the cytoskeleton to the extracellular matrix.[12] The C terminus associates with syntrophins and dystrobrevins.[13]

Current treatments for DMD and BMD include corticosteroids, support of respiratory problems with ventilation-assisted devices, physical therapy, and surgery for scoliosis.[14] Corticosteroids have been demonstrated to prolong ambulation and lifespan of patients.[15,16] More recently, antisense oligonucleotides (ASOs) to restore the reading frame of dystrophin have become a treatment option for some patients with mutations that are amenable to exon skipping.[2] ASOs must be designed to target a certain set of mutations; therefore, this treatment option needs to be tailored.[17] While more potent exon-skipping strategies are in development, current ASOs require weekly intravenous injections that result in very little dystrophin expression compared with those in healthy individuals.[18–21]

A major challenge in the field is addressing the heart problems that impact both DMD and BMD patients. The lack of dystrophin

Received 17 October 2025; accepted 1 July 2026;
https://doi.org/10.1016/j.omta.2026.201801.

**Correspondence:** Asuka Eguchi, Department of Physiology and Biophysics, University of California, Irvine, Irvine, CA 92697, USA.
**E-mail:** asuka.eguchi@uci.edu

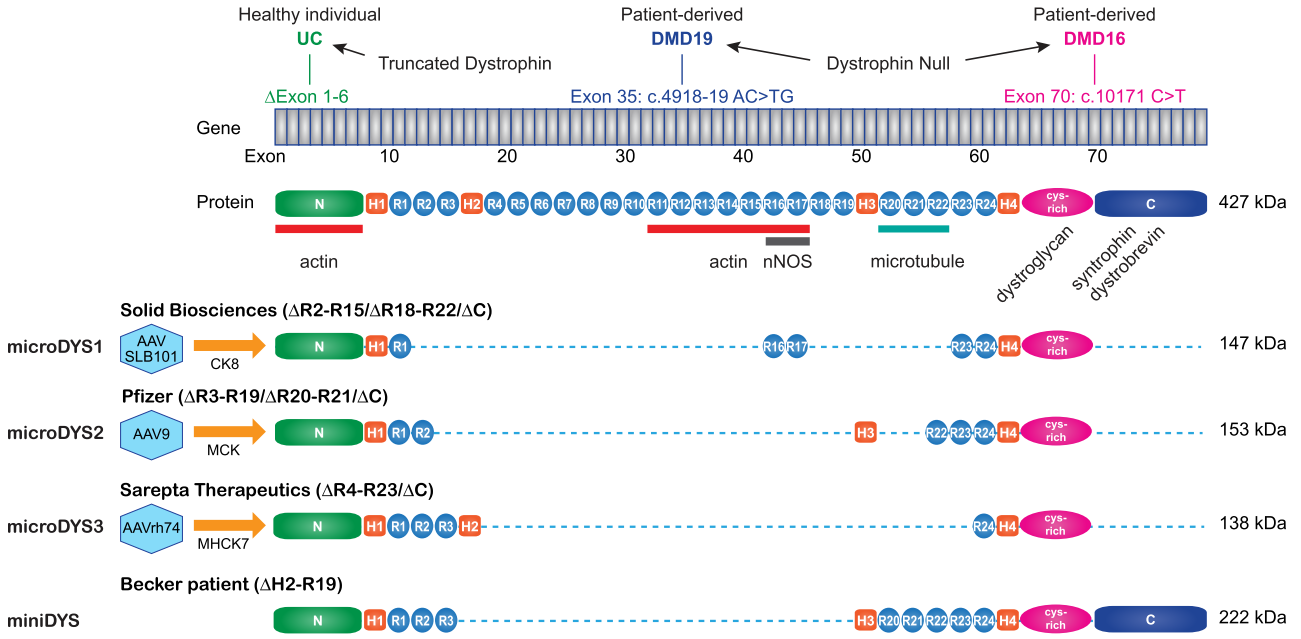


**Figure 1. Mutations in dystrophin and transgenes**

Schematic shows mutations in the diseased lines. The UC1015.6 line has a CRISPR-edited mutation that produces a truncated dystrophin variant lacking the N terminus. DMD19 and DMD16 are patient-derived lines bearing nonsense mutations. Domains of dystrophin are highlighted along with transgenes and sponsors of the clinical trials associated with the transgene. miniDYS is derived from a case study of a BMD patient. nNOS, nitric oxide synthase.

expression in the heart leads to contractile dysfunction and a compromised plasma membrane, resulting in excess calcium in cardiomyocytes (CMs) and premature CM loss in the heart.[14] These CMs are replaced with fat and fibrotic scar tissue, eventually leading to the development of dilated cardiomyopathy.[14] Angiotensin receptor neprilysin inhibitors (ARNIs), prescribed to reduce the mechanical load on the heart and reduce blood pressure, extend lifespans but do not prevent the onset of cardiomyopathy.[22] This cardiomyopathy is difficult to model; the *mdx* mouse, the most commonly used dystrophin-null animal model, exhibits cardiac problems only at a geriatric age, following a very different trajectory compared with DMD patients who die in the second or third decade of life.[23]

To better model cardiac complications in the molecular context of human cells, we use CMs differentiated from human induced pluripotent stem cells (iPSCs). DMD iPSC-CMs exhibit key disease phenotypes including poor calcium handling, impaired contractile function, and reduced viability.[24,25] This platform enables investigation of the therapeutic efficacy of various gene therapy strategies. Restoration of dystrophin expression is particularly difficult by current gene therapy methods as the dystrophin transcript spans 14 kb,[8] far exceeding the 4.7 kb packaging limit of AAVs.[26] Smaller, synthetic variants of dystrophin, called microdystrophins (Figure 1), have advanced to clinical trials (NCT03368742 for microDYS1, NCT04281485 for microDYS2, NCT05096221 for microDYS3, and NCT05693142), and Elevidys received FDA approval in 2023.[27] In dystrophic mouse models, these microdystrophins properly localize at the sarcolemma, reduce muscle damage, and improve force generation in the skeletal muscle.[28–31] In female geriatric *mdx* mice, the ΔR4-R23/ΔC microdystrophin (microDYS3) reduced fibrosis and improved ejection fraction.[32] In dobutamine-challenged *mdx* mice, the ΔR4-R23/ΔC microdystrophin (microDYS3) prevented cardiac pump failure.[33] While these data demonstrate therapeutic efficacy in preclinical models, it is unknown if these microdystrophins are effective in delaying the onset of dilated cardiomyopathy in patients because it can take several years for heart complications to develop, and no study has reported patient outcomes with respect to heart function.

These synthetic microdystrophin variants were inspired by a BMD patient who retained the ability to walk even at 61 years of age, highlighting the functional nature of his dystrophin variant in the skeletal muscle, diaphragm, and the heart.[34,35] This patient's dystrophin variant, called minidystrophin (miniDYS), is a truncated variant that is half the size of dystrophin.[34] In this study, we compared three microdystrophins (microDYS1, microDYS2, and microDYS3) with miniDYS in DMD iPSC-CMs. Our results suggest that the larger miniDYS may have better outcomes in diseased CMs than the microdystrophins.

## RESULTS

### Designs of the transgenes were tested in three iPSC lines bearing different DMD mutations

We used three human iPSC lines with different DMD mutations, alongside isogenic controls without the dystrophin mutation

**Table 1. iPSC lines and mutational status**

| iPSC line | Mutation type | Dystrophin | Description |
|---|---|---|---|
| UC3.4 | none | full-length | healthy control |
| UC1015.6 | CRISPR-edited | truncated | DMD (Δexons 1–6) |
| DMD19 iso | CRISPR-corrected | full-length | healthy control |
| DMD19 | patient-derived | null | DMD (c.4918_4919AC>TG) |
| DMD16 iso | CRISPR-corrected | full-length | healthy control |
| DMD16 | patient-derived | null | DMD (c.10171C>T) |

Healthy lines are in black, and DMD lines are italicized. UC3.4 was derived from a healthy individual. UC1015.6 is a CRISPR-edited line where the deletion of c.19 in UC3.4 results in the expression of a truncated dystrophin missing exons 1–6. DMD19 and DMD16 are patient-derived lines that are dystrophin-null due to nonsense mutations. DMD19 iso is a CRISPR-corrected healthy isogenic control line for DMD19. DMD16 iso is a CRISPR-corrected healthy isogenic control line for DMD16.

(Figure 1; Table 1).[36–39] The UC3.4 cell line was derived from a healthy individual.[39] A CRIPSR-edited mutation caused deletion of nucleotide 19 in the coding sequence, resulting in the UC1015.6 line.[39] This specific mutation results in the expression of a truncated dystrophin that lacks the N terminus.[39] Such mutations are associated with the early onset of dilated cardiomyopathy.[10] Both the DMD19 and DMD16 iPSC lines were derived from DMD patients with nonsense mutations, resulting in a lack of dystrophin expression. These nonsense mutations have matching isogenic controls where the dystrophin mutation is corrected. Mutational status of the cell lines was verified through Sanger sequencing (Figure S1). We validated that the iPSCs express the pluripotency markers OCT4, SOX2, NANOG, and TRA-1-60 (Figure S2).

The microdystrophins that have advanced to clinical trials are depicted in Figure 1, which also highlights the domains interacting with specific proteins. All the microdystrophins have the N terminus, hinge 1, spectrin-like repeats 1 and 24, hinge 4, and the cysteine-rich domain. Unique domains of the microdystrophins include spectrin-like repeats 16 and 17 to recruit neuronal nitric oxide synthase (microDYS1),[30,40] spectrin-like repeat 22 to bind microtubules (microDYS2),[41] and spectrin-like repeat 3 that interacts with the plasma membrane[42] and hinge 2 (microDYS3). To benchmark these microdystrophins, we included miniDYS, a larger variant discovered in a BMD patient who lived into his seventies.[34,35]

To focus on the transgene design, we chose to make the transgene the only variable in the experimental design (Figure 2A), unlike the clinical trials that implement different delivery capsids and promoters (Figure 1). We delivered the microdystrophins and miniDYS in lentivirus under the control of a cardiac troponin T (TNNT2) promoter.[43] We included an empty vector control containing a zeocin resistance gene (Figure 2A). For the gene therapies, a zeocin resistance gene separated by a T2A self-cleaving peptide was incorporated into each construct. The zeocin resistance gene enabled simultaneous purification of iPSC-CMs that were transduced with lentivirus and the CM population, as the transgenes were under control of a cardiac-specific promoter. Because the efficiency of differentiation from iPSCs can vary among different lines and replicates, zeocin selection allowed us to enrich for the CM population.

We differentiated human iPSCs into iPSC-CMs by modulating the Wnt pathway.[44] By day 8–14 of differentiation, iPSC-CMs underwent spontaneous contraction and continued to contract until day 38, the last time point of our study. On day 10 of differentiation, we transduced iPSC-CMs with an empty vector control, microDYS1, microDYS2, microDYS3, or miniDYS (Figures 2A and 2B). On days 18 and 19, we performed zeocin selection, and on day 30, we conducted assays. Immunostaining of TNNT2 on day 30 iPSC-CMs showed differentiation into CMs (Figures 2C, S3A, and S4A). Gene therapy did not cause any obvious differences in spontaneous contractions (Videos S1, S2, and S3). We previously reported that DMD iPSC-CMs exhibit morphological defects, including reduced cell size and reduced nuclear size.[24] Changes in nuclear morphology have also been reported in the hearts of DMD patients.[45] In DMD19 iPSC-CMs, none of the gene therapies affected cell size, while microDYS2 rescued the median nucleus size from 92 μm (interquartile range [IQR], 72–113 μm) in DMD empty iPSC-CMs to 100 μm (IQR, 80–123 μm) (Figures 2D and 2E). No positive outcomes were observed in the UC iPSC-CMs (Figures S3B and S3C). All three microdystrophins improved cell size in DMD16 iPSC-CMs. The median cell size of 1,010 μm (IQR, 585–1,494 μm) in DMD empty iPSC-CMs was rescued to 1,285 μm (IQR, 836–2,128 μm) by microDYS1, to 1,397 μm (IQR, 944–2,041 μm) by microDYS2, and to 1,269 μm (IQR, 832–2,068 μm) by microDYS3 (Figure S4B). As for nuclear size, the median nuclear size improved from a median of 105 μm (IQR, 83–131 μm) in DMD empty iPSC-CMs to 123 μm (IQR, 99–156 μm) by microDYS1 and 122 μm (IQR, 101–155 μm) by microDYS3 (Figure S4C). These results suggest that the microdystrophins can alter the cell morphologies to resemble healthy cells; however, these outcomes are variable among different genetic backgrounds.

### Microdystrophins and miniDYS alter the transcriptional profile of DMD iPSC-CMs

Transcriptional profiling by other groups has shown that the expression of proteins involved in calcium handling, contraction, and adhesion to the extracellular matrix is disrupted in DMD iPSC-CMs.[46,47] We hypothesized that gene therapy would restore the proper expression of these pathogenic gene signatures. To characterize the global transcriptional profiles of pluripotent cells and treated iPSC-CMs, we performed bulk RNA sequencing (RNA-seq) on iPSCs and day 30 iPSC-CMs. Hierarchical clustering and principal-component analysis (PCA) in the DMD19 background confirmed the distinct gene signatures of iPSCs and iPSC-CMs (Figures 3A and S5A). While the control empty iPSC-CMs clustered together, the replicates for the DMD empty iPSC-CMs did not (Figures 3A and S5B). When we took the average of the normalized gene counts for each condition and

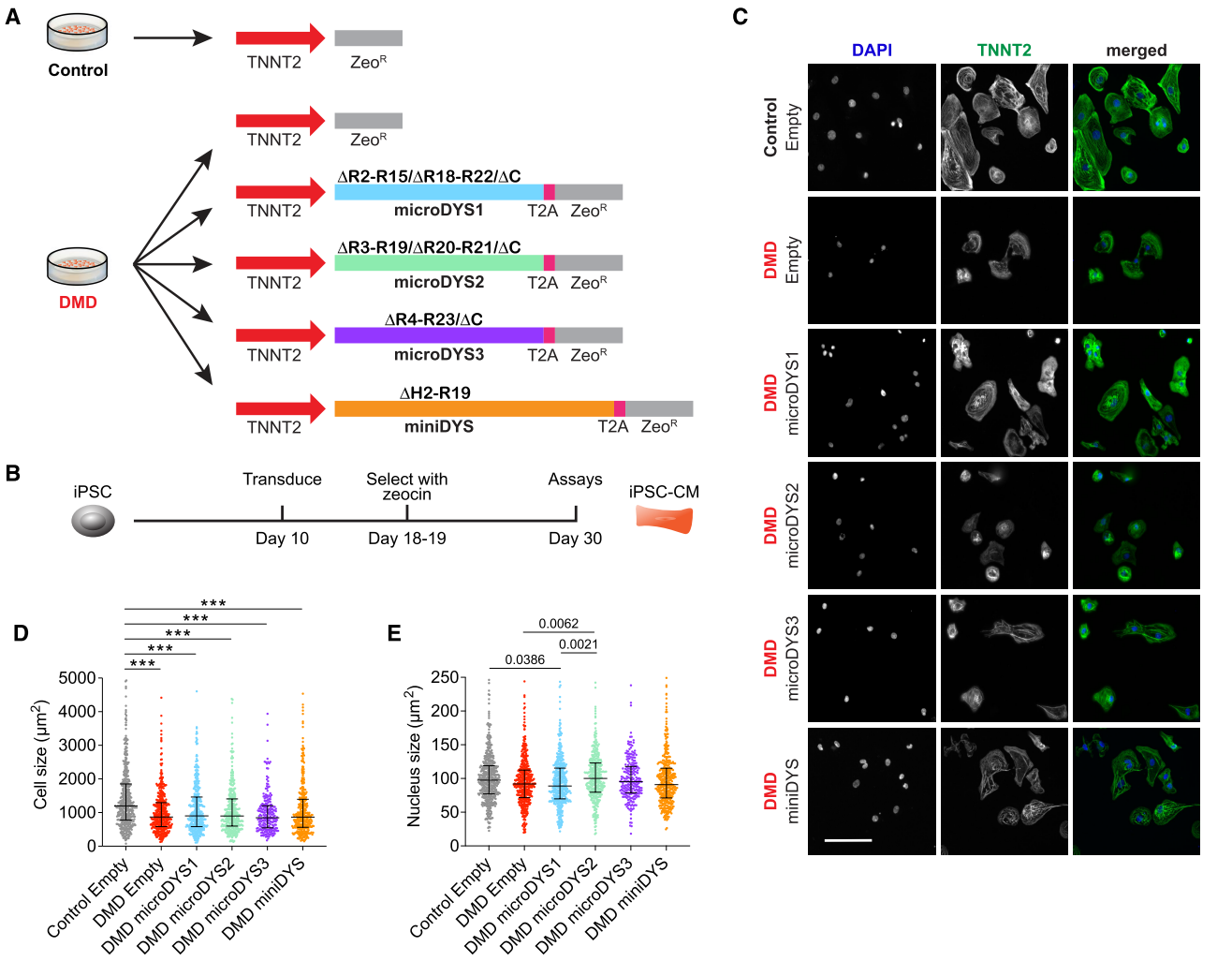


**Figure 2. Experimental design and differentiation to CMs**

(A) Lentiviral constructs and conditions. The empty vector contains a zeocin resistance gene driven by a cardiac troponin T promoter. The gene therapy constructs comprise a transgene and a zeocin resistance ($Zeo^R$) gene separated by a T2A self-cleaving peptide. (B) Experimental timeline; iPSCs differentiated into CMs and were transduced on day 10 of differentiation. Selection with zeocin enriches for iPSC-CMs expressing transgenes. Assays were performed on day 30. (C) TNNT2 immunostaining of DMD19 iPSC-CMs. DAPI marks nuclei. Scale bar is 100 μm. (D and E) Cell size (D) and nucleus size (E) quantification of DMD19 iPSC-CMs. Data represent median with interquartile ranges from 4–7 differentiation experiments. $n$ = 225–457 cells. One-way ANOVA and Kruskal-Wallis test for post-hoc at $p < 0.05$. ***$p < 0.001$.

examined the PCA plots, we found that the microdystrophin and miniDYS-treated conditions clustered together and were distinct from the control empty and DMD empty iPSC-CMs (Figure 3B). We also confirmed the reduced expression of dystrophin (gene symbol: DMD) in DMD empty iPSC-CMs compared with the control empty iPSC-CMs (Figures 3C and S6). At the transcript level, we observed trends in elevated dystrophin levels, but these differences were not statistically significant (Figures 3C and S7A–S7M). Western blotting for dystrophin confirmed expression of the transgenes (Figures 3D, S8A and S8B).

We performed differential gene expression analysis and found that cardiac differentiation and development genes were differentially expressed between the control empty and DMD empty iPSC-CMs (Figure 3E), consistent with the findings of other groups.[46,47] When we compiled a list of all differentially expressed genes (DEGs) for pairwise comparisons between control empty and DMD empty iPSC-CMs, we found a total of 730 DEGs that clustered into four groups (Figure 3F; Tables S1 and S2). The most drastic differences among conditions were between the control empty and DMD empty iPSC-CMs with 385 DEGs (Table S1). Because the gene therapy treatments clustered together, we examined the overlap of these DEGs among treatments and found that most of the shared transcripts were common among downregulated genes (Figures S9A–S9F and S10F; Table S1). There were only two transcripts that were similar between the control empty and the gene therapy treatments in DMD

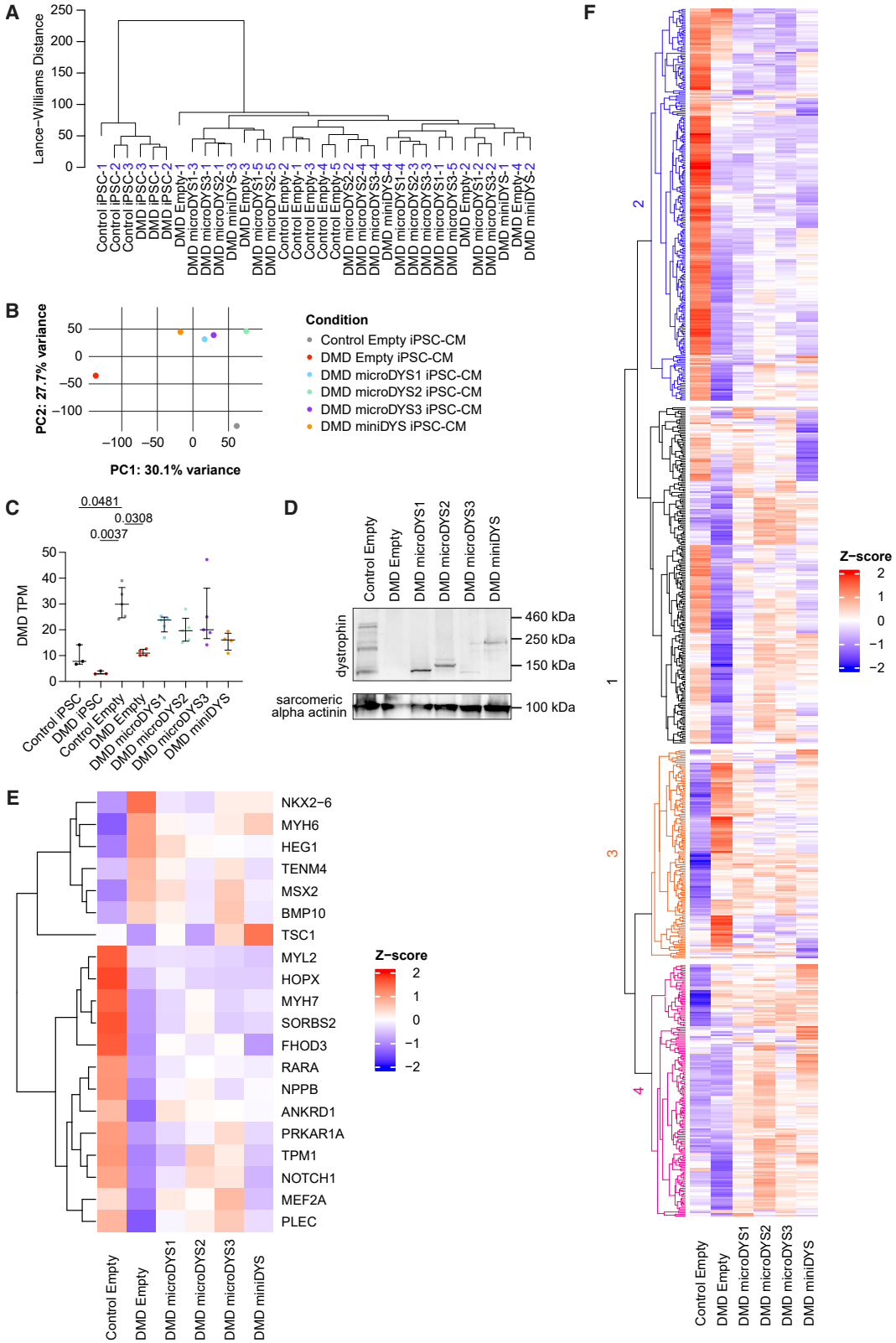


*(legend on next page)*

iPSC-CMs (Table S1). Creatine kinase (CKM) was downregulated in both control empty and DMD microDYS2 iPSC-CMs. Neural cell adhesion molecule 1 (NCAM1) was upregulated in both control empty and DMD miniDYS iPSC-CMs.

Gene ontology (GO) enrichment analysis of the clusters in Figure 3F revealed overlapping GO terms. Cluster 1, which included genes that were downregulated in DMD iPSC-CMs and impacted by gene therapy, had GO terms related to extracellular matrix proteins (COL27A1, FN1, MMP2, and TGFB3) (Figure S11A; Table S3). Cluster 2, which also included genes downregulated in DMD iPSC-CMs and slightly impacted by gene therapy, had GO terms related to muscle contraction (CAVIN4, MYH7, MYL2, and TNNT2) (Figure S11B; Table S3). Cluster 3, which includes genes that were upregulated in DMD iPSC-CMs, had GO terms related to the sarcomere (ANK2, BMP10, DES, and LDB3) (Figure S11C; Table S3). Cluster 4, which highlighted genes that were uniquely upregulated by gene therapy, comprised GO terms related to the cellular stress pathways (CAT, CYGB, ENG, and MB) (Figure S11D; Table S3).

In the comparison of control empty and DMD empty iPSC-CMs, GO terms were found to be related to extracellular matrix proteins (FBLN2, NCAM1, MMP2, and LAMA1) (Figure S11E; Table S4). Likewise, treatment with microDYS1 in comparison to DMD empty iPSC-CMs showed GO terms related to the extracellular matrix (FN1 and MMP2) (Figure S11F; Table S4). "Regulation of cellular response to growth factor stimulus" and “cell-substrate adhesion” were the GO terms associated with microDYS2 treatment with DMD empty iPSC-CMs as a reference (MAP4K4, ACTN3, ELAPOR2, and SPRY4) (Figure S11G; Table S4). After treatment with microDYS3 or miniDYS, GO terms that were impacted included small GTPase-mediated signal transduction (GNB1, OBSCN, and TNK2) (Figures S11H and S11I; Table S4). We found that treatment with the microdystrophins or miniDYS induced marked changes to the transcriptional profiles of DMD iPSC-CMs; however, these transcriptional profiles were still distinct from those of control iPSC-CMs.

### MiniDYS and microDYS3 improve calcium-handling deficits in DMD iPSC-CMs

To test the functional efficacy of gene therapy in DMD iPSC-CMs, we performed ratiometric calcium imaging. We and others have demonstrated that DMD iPSC-CMs exhibit arrhythmias and aberrant calcium handling.[24,25,48,49] To assess the effect of gene therapy on arrhythmias, we seeded iPSC-CMs as single cells on day 27 of differentiation onto micropatterns with a 7:1 length:width aspect ratio, an elongated shape that promotes parallel alignment of myofibrils.[50] On day 30, we performed ratiometric calcium imaging with Fura Red. We paced iPSC-CMs at 1 Hertz (Hz) to induce contraction at 1-s intervals and classified the calcium transients as non-arrhythmic or arrhythmic (Figure 4A). We found that 66% of DMD empty iPSC-CMs were arrhythmic as compared with 23% of control empty iPSC-CMs in the DMD19 background (Figure 4B; Table S5; chi-squared test, $p = 0.002$). Treatment with microDYS1, microDYS2, and microDYS3 did not significantly reduce arrhythmia. Only treatment with miniDYS significantly decreased the number of arrhythmic cells to 33% in the DMD19 line (Figure 4B; Table S5; chi-squared test, $p = 0.040$). In the UC background, 58% of DMD empty iPSC-CMs were arrhythmic relative to 21% of control empty iPSC-CMs (Figure S12A; Table S5; chi-squared test, $p = 0.002$). While treatment with gene therapy reduced the percentage of arrhythmic events to 42%–43%, none of the treatments were statistically significant. In the DMD16 background, we observed no differences between the control and DMD empty iPSC-CMs with respect to the frequency of arrhythmia (Figure S13A; Table S5; chi-squared test).

Next, we examined specific parameters of calcium transients, including time-to-peak, peak frequency, and peak duration (Figure 4A). Typically, a subset of DMD iPSC-CMs exhibit a higher peak frequency, even though they are being paced at 1 Hz. While peak frequencies between the control empty and DMD empty were not statistically significant, the IQRs for all lines were greater for DMD empty (Figures 4C, S12B, and S13B). In the DMD19 background, microDYS3 significantly reduced the peak frequency from a median of 1.04 s (IQR, 0.95–1.77 s) in the DMD empty to 0.99 s (IQR, 0.97–1.02 s) (Figure 4C). As the peak frequency increased, time-to-peak tended to be faster in DMD empty iPSC-CMs. While not statistically significant in the DMD19 and UC backgrounds, time-to-peak was significantly faster in the DMD16 background, with a median of 0.32 s (IQR, 0.23 s–0.39 s) in DMD empty compared with 0.39 s (IQR, 0.33 s–0.44 s) in the control empty (Figures 4D, S12C, and S13C). For the DMD19 line, microDYS2 significantly exacerbated time-to-peak by shortening it from 0.28 s (IQR, 0.21–0.35 s) in DMD empty to 0.22 s (IQR, 0.17–0.26 s) (Figure 4D). For the UC line, miniDYS corrected the time-to-peak from a median time of 0.33 s (IQR, 0.24–0.40 s) in the DMD empty to 0.37 s (IQR, 0.28–0.43 s) (Figure S12C). Because the peak frequency is higher in DMD, peak duration is typically shorter in DMD empty iPSC-CMs. Peak duration shortened from 1.00 s (IQR, 0.998–1.002 s) in control empty to 0.97 s (IQR, 0.56–1.001 s) in DMD empty in the DMD19 background, and the

**Figure 3. Gene expression profiles of iPSC-CMs after gene therapy**

(A) Hierarchical clustering of bulk RNA-seq of the DMD19 line shows that iPSCs and iPSC-CMs cluster separately. (B) Principal-component analysis (PCA) of DMD19 iPSC-CMs. The gene expression profiles of biological replicates were averaged before PCA was completed. (C) Quantification of dystrophin expression in iPSCs and iPSC-CMs. Dystrophin was quantified at the gene level. Data from each condition represent median with interquartile ranges from 3–5 differentiation experiments. One-way ANOVA and Kruskal-Wallis test for post-hoc comparison at $p < 0.05$. (D) Western blot of dystrophin levels, with GAPDH as a loading control in DMD19 D30 iPSC-CMs. Expected sizes are 427 kDa for full-length dystrophin, 147 kDa for microDYS1, 135 kDa for microDYS2, 138 kDa for microDYS3, 222 kDa for miniDYS, and 37 kDa for GAPDH. (E) Heatmap of differentially expressed genes (DEGs) related to cardiac development and differentiation. (F) Heatmap of all DEGs from pairwise comparisons. DEGs separate into four clusters, determined by unbiased hierarchical clustering. DEGs were defined with a cutoff value of absolute $\log_2$ fold change > 1 and FDR < 0.05.

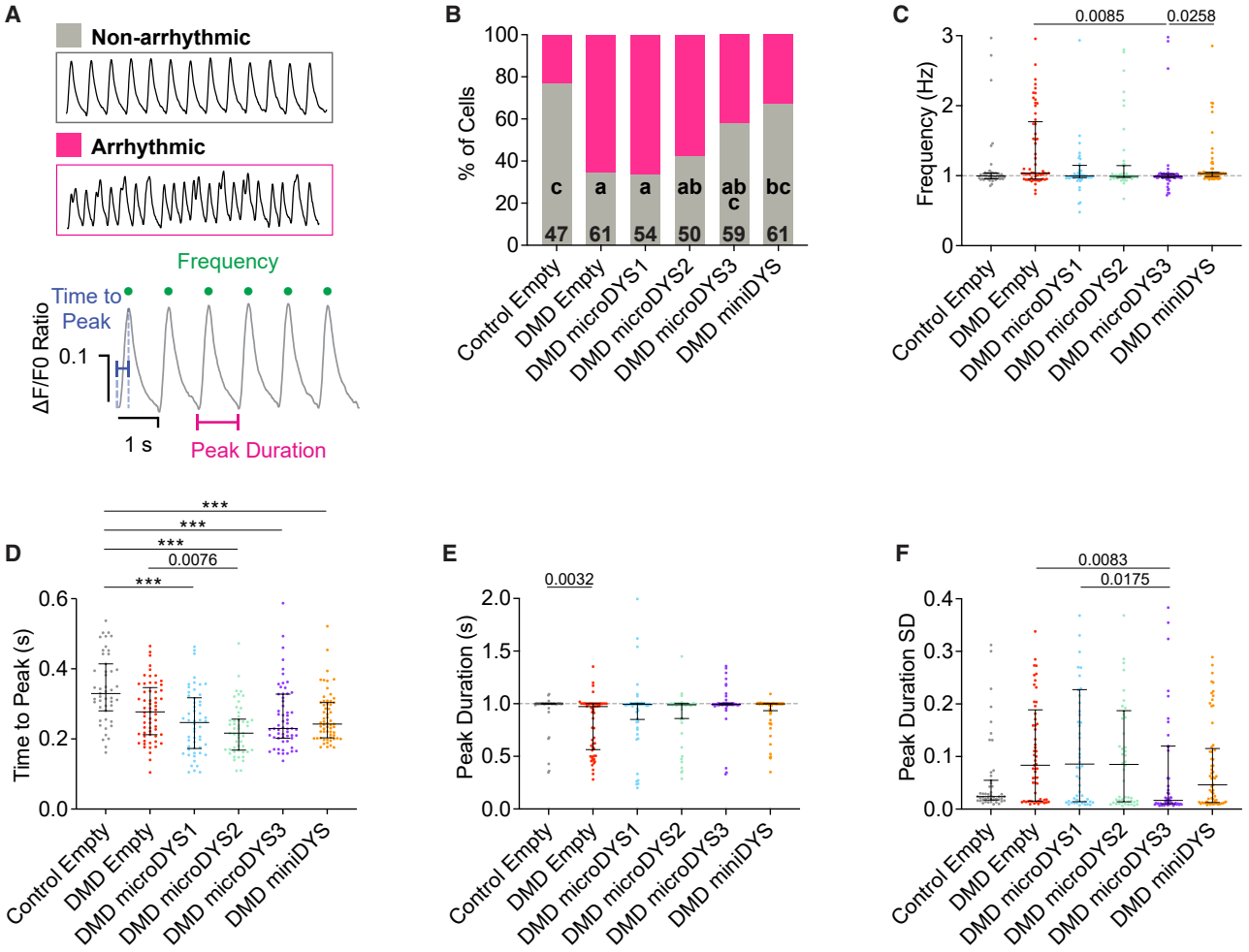


**Figure 4. Assessment of arrhythmia by calcium imaging in iPSC-CMs after gene therapy**

(A–F) Ratiometric calcium imaging was performed on day 30 iPSC-CMs paced at 1 Hertz. (A) Classification of calcium transients in single cells and parameters of calcium handling. Non-arrhythmic traces exhibited 1-s peak durations. Arrhythmic traces showed deviations from the 1-s peak durations or double spiked peaks, indicative of early afterdepolarization events. Frequency is the rate of oscillations per second. Time-to-peak is the duration from minimum to maximum. Peak duration is the duration from minimum to minimum. (B) Frequency of arrhythmia in DMD19 iPSC-CMs. The percentage of cells is defined as the number of cells in a given category divided by the total number of cells. A chi-square test was used to determine significance. Different letters indicate statistical significance at $p < 0.05$. (C–F) Frequency (C), time-to-peak (D), peak duration (E), and peak duration standard deviation (F) in DMD19 iPSC-CMs. Data represent median with interquartile ranges from 5–6 differentiation experiments with 47–61 cells per condition. One-way ANOVA and Kruskal-Wallis test for post-hoc comparison at $p < 0.05$. ***$p < 0.001$.

peak durations were not significantly different between the other two lines (Figures 4E, S12D, and S13D). We observed a higher standard deviation for peak duration in DMD empty that in the control empty iPSC-CMs in the UC background (Figure S12E). Gene therapies had no significant effect on standard deviation of peak duration for the other lines (Figures 4F and S13E).

Examination of the RNA-seq results suggests that miniDYS improves calcium handling in DMD iPSC-CMs because a unique set of genes are expressed in this condition. A collection of transcripts related to the cytoskeleton, transcription, ion regulation, and metabolism could explain the reduction of arrhythmia with miniDYS (Figure S14A; Table S6). For microDYS3, there was a smaller set of uniquely expressed genes, including those related to the cytoskeleton, cardiac development, and metabolism (Figure S14B; Table S6). These unique signatures may contribute to the reduction in peak frequency. Collectively, these data suggest that miniDYS and microDYS3 treatments have a positive outcome on calcium handling; however, these results were highly variable among lines, suggesting that the interventions may depend on the genetic background or the type of mutation.

### MiniDYS improves the viability of DMD iPSC-CMs

The initiating event in the progression to dilated cardiomyopathy is premature CM loss in the DMD heart. Because the DMD iPSC-CMs

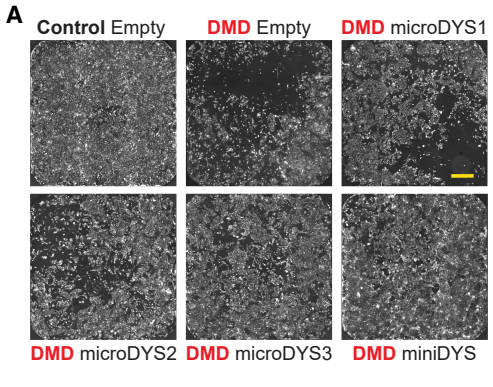


**Figure 5. Impact of gene therapy on viability of DMD iPSC-CMs**

(A) Representative wells stitched from 12 images of DMD19 iPSC-CMs loaded with TMRM, a dye that measures the mitochondrial membrane potential, on day 38. Scale bar is 500 μm. (B) Quantification of survival for DMD19 iPSC-CMs. Cell survival was determined by dividing the live cell area on day 38 by the live cell area on day 30. Data represent the median with interquartile ranges from 9 differentiation experiments. One-way ANOVA and Kruskal-Wallis test for post-hoc comparison at $p < 0.05$.

exhibited continuous contraction from day 14 onward, these cells experienced membrane fragility due to the lack of dystrophin and contraction-induced injury. Human iPSC-CMs provide an excellent model to recapitulate this premature cell death as we have previously shown that DMD iPSC-CMs die prematurely compared with control iPSC-CMs.[24] To determine if microdystrophins or miniDYS can restore viability in DMD iPSC-CMs, we compared the survival of iPSC-CMs over time (Figure 5A). Using a dye that measures the mitochondrial transmembrane potential, tetramethylrhodamine methyl ester (TMRM), we measured cell viability on days 30 and 38 of differentiation. By tracking the same cells over time, we were able to assess the percentage of cells that survived over the period of 8 days. For DMD19, the microdystrophins improved the median cell viability to 79%–86% (IQR, 65%–92%) from 66% (IQR, 44%–75%) in DMD empty iPSC-CMs, and these differences were not statistically significant (Figures 5A and 5B). On the other hand, miniDYS significantly improved the median cell viability to 88% (IQR, 77%–94%). For the UC line, the microdystrophins improved the median cell viability to 85%–86% (IQR, 78%–93%) from 70% (IQR, 65%–74%) in DMD empty iPSC-CMs (Figures S15A and S15B). These differences were not statistically significant. As in the DMD19 line, miniDYS rescued DMD iPSC-CMs from death by improving their median viability to 91% (IQR, 90%–95%) in the UC background. For DMD16, the microdystrophins improved the median cell viability from 68% (IQR, 36%–75%) in DMD empty to 66%–74% (IQR, 62%–92%) and miniDYS to 87% (IQR, 71%–92%); however, none of the comparisons were significant (Figures S15C and S15D). These results suggest that miniDYS has the greatest potential to rescue DMD CMs from premature death as we observed significant rescue in two of three lines. In-depth analysis of the gene signatures unique to miniDYS demonstrated that the expression of genes related to the cytoskeleton, apoptosis, oxidative stress, and transcription may be contributing to the therapeutic efficacy of miniDYS (Figure S14A; Table S6).

## DISCUSSION

Investigating the therapeutic effect of microdystrophins on the DMD heart has been challenging to model in animal studies and difficult to ascertain from clinical trials that have not spanned a period long enough to assess cardiac benefit. Our study modeled cardiac complications in DMD in the molecular context of human cells by using three lines bearing different dystrophin mutations in distinct genetic backgrounds. We also employed matching isogenic control cell lines to benchmark therapeutic efficacy against full-length dystrophin expression. In this study, we focused on the transgene design and standardized other variables that affect transgene expression, such as vector type and promoter. Inclusion of a zeocin resistance gene enabled enrichment of the CM population, as we used a cardiac-specific promoter, and allowed us to purify the cells that expressed the transgene. Despite standardizing the vector, we consistently observed a reduced expression of microDYS3 compared with the other transgenes (Figures 3D, S8A and S8B). Translational control, mRNA stability, or epigenetic silencing may be affecting microDYS3 expression. When translated to the clinic, transduction efficiency will be limited by tropism of the delivery vector, but we chose to examine a scenario in which all the cells were expressing the transgene. In this context, we demonstrate that the microdystrophins partially rescue disease characteristics in DMD iPSC-CMs, including reduced cell size in the DMD16 line. The smaller cell size we observed in DMD iPSC-CMs is likely a developmental defect as the CMs differentiated from iPSCs are more fetal in nature. Although the morphological differences we observed between the control empty and DMD empty iPSC-CMs may not recapitulate similar differences in patients, we reasoned that we could assess the role of the dystrophin variants in rescuing this developmental defect.

As a point of comparison, we transduced miniDYS, which is much larger than any of the microdystrophins. Improvement of aberrant calcium handling by the microdystrophins was highly variable and dependent on the genetic background. While miniDYS rescued arrhythmic events in the DMD19 background, microDYS3 rescued peak frequency in the same line. In the DMD16 background, miniDYS improved time-to-peak. We did not observe consistent outcomes among different lines, suggesting that the therapeutic efficacy may be dependent on the type of mutation or variations in other genes that affect cardiac function. Indeed, one of the diseased lines in our study, UC1015.6, expresses a truncated dystrophin missing the N terminus encoded by the first six exons of dystrophin.[39] We used this

line because we and others have observed disease phenotypes,[24,38,39] but such truncated variants may compete for occupancy at the dystroglycan complex as both the transgene and the endogenous variant include the cysteine-rich domain that associates with the dystroglycan complex. Competition between endogenous dystrophin and the transgene may extend beyond association with the dystroglycan complex. Thus, the phenotypes observed in the UC line may be different from the dystrophin-null lines, DMD19 and DMD16, due to differences in endogenous expression.

Bulk RNA-seq, quantitative reverse-transcription PCR (RT-qPCR), and western blotting confirmed dystrophin expression in control empty iPSC-CMs and the lack of expression in DMD empty iPSC-CMs. Expression at the transcript level of microDYS1, microDYS2, microDYS3, and miniDYS in DMD empty iPSC-CMs was less than that in control empty iPSC-CMs, and further examination of the 5′ and 3′ untranslated regions (UTRs) is warranted as the lentiviral constructs did not include native UTRs or a poly(A) tail. Global transcriptional profiling revealed that DMD empty iPSC-CMs exhibited pathogenic signatures compared with control empty iPSC-CMs with aberrant expression of cardiac development and collagen-containing extracellular matrix genes. While transduction with the transgenes altered the transcriptional profiles of DMD iPSC-CMs, the cells subjected to various gene therapies were more similar to each other but remained distinct from DMD empty and control empty iPSC-CMs, suggesting that dystrophin may play an important role in differentiation and that the lack of dystrophin has lasting effects on cellular function.

Importantly, our data showed that miniDYS performs better than the microdystrophins in rescuing poor viability of DMD iPSC-CMs. Progression to dilated cardiomyopathy begins with the premature loss of CMs in the DMD heart. Therefore, it is imperative that gene therapy prolongs the survival of DMD CMs to sustain cardiac function in patients. While the microdystrophins trended toward rescuing poor viability, the results were not statistically significant. In our experiments, we included six different conditions in three genetic backgrounds, which makes our study comprehensive. At the same time, the number of conditions reduced the statistical power to detect differences with the sample sizes that were feasible for these labor-intensive experiments (Table S7). One limitation of our study is the immature nature of the iPSC-CMs, which have disorganized myofibrils, rely on glycolysis for energy, and lack mitochondria.[51] We used media deficient in glucose and supplemented with lactate to promote maturation.[52] In addition, for calcium imaging experiments, we micropatterned the iPSC-CMs to a physiologically elongated shape that promotes parallel alignment of the myofibrils[51] and electrically stimulated the iPSC-CMs to measure arrhythmic events in response to pacing. While the iPSC-CMs are not fully mature, we were able to measure clear differences between the control empty and DMD empty iPSC-CMs with respect to morphology, arrhythmic events, and viability, which enabled us to use these readouts to assess therapeutic efficacy of the microdystrophins.

Our findings highlight the necessity to explore dystrophin variants that are larger than the microdystrophins. Systems employing split inteins to deliver larger variants of dystrophin split into two or three independent AAV genomes have been successful at restoring dystrophin expression and improving skeletal muscle and heart function in *mdx* mice.[53–55] Because male *mdx* mice have the average lifespan of 21.5 months and do not exhibit cardiac problems until 21 months of age, assessment of microdystrophin gene therapy as an effective way to delay the onset of cardiac complications has been challenging.[56,57] In more severe dystrophic models, outcomes of microdystrophin gene therapy have been mixed. In *mdx*/*utrophin* double knockout (dKO) mice, microDYS3 improved fractional shortening and enhanced their survival.[58] By contrast, microDYS3 reduced the ejection fraction and shortened the lifespan of D2.*mdx* mice compared with untreated controls, underscoring the potential for microdystrophin to have toxic effects.[59] Hinge 2 in microDYS3 has been reported to be problematic, and replacement of hinge 2 with hinge 3 corrected the issues that microDYS3 had on the myotendinous junction and neuromuscular junction.[60] This variant of microDYS3, ΔH2-R19/ΔR20-R23/ΔC (μDysH3), improved ejection fractions of Fiona/dKO mice that are deficient in dystrophin and utrophin but express utrophin in the skeletal muscles only.[61]

In the broader context of AAV-mediated gene therapy, safety remains a concern. Patients generally receive $>10^{14}$ vector genomes/kg of body weight, a viral load that mounts a strong immune response. Two non-ambulatory patients receiving Elevidys as well as two patients from the Pfizer clinical trial have died from serious adverse effects of gene therapy. Because Pfizer did not meet their primary endpoint of improvement on the North Star Ambulatory Assessment (NSAA) score, their phase 3 study ended in 2024 (clinical trial ID: NCT04281485).[62] Despite not meeting their primary endpoint of improvement on the NSAA score, Sarepta Therapeutics received accelerated approval for Elevidys in 2023, and the label was expanded to all age groups in 2024 (clinical trial ID: NCT05096221).[63,64] Testing of delivery vehicles, such as myotropic AAVs that deliver effectively to human cells, is an important avenue of exploration to reduce the viral load necessary for transgene expression, particularly when two independent vectors are necessary for a larger payload.

## MATERIALS AND METHODS

### iPSCs

All human iPSC lines were approved by and used in accordance with the Human Stem Cell Research Oversight Committee at the University of California, Irvine.

### iPSC differentiation into CMs

iPSCs were seeded onto Matrigel (Fisher, Waltham, MA; CB-40230C)-coated plates and were cultured in Nutristem (Reprocell, Beltsville, MD; 01–0005) medium, which was changed daily. iPSCs were cultured to 70%–90% confluency and then cultured in RPMI 1640 supplemented with 1X B27 minus insulin (Invitrogen, Waltham, MA; A1895601) and 4–6 μM CHIR-99021 (Sigma-Aldrich,

St. Louis, MO; SML1046). Two days later, the cells were refreshed with RPMI 1640 supplemented with 1× B27 minus insulin and 5 μM IWR-1 (Sigma-Aldrich; I0161). Another two days later, the cells were refreshed with RPMI 1640 supplemented with 1× B27 (Invitrogen; 17-504-044) and maintained for 4 days, with medium changes every two days. On day 10 of differentiation, iPSC-CMs were transduced with an empty vector lentiviral control or microDYS1, microDYS2, microDYS3, or miniDYS with 8 μg/mL polybrene (Sigma-Aldrich; TR-1003-G). From this point forward, iPSC-CMs were refreshed every two days with RPMI 1640 minus glucose supplemented with 1× B27 and 4 mM lactate (Sigma-Aldrich; 71718). On day 14, iPSC-CMs were replated onto Matrigel-coated plates with Accutase (Fisher; NC9464543) and TrypLE (Invitrogen; A1217701) into RPMI 1640 minus glucose supplemented with 1× B27, 4 mM lactate, 5% KnockOut Serum Replacement (KSR) (Invitrogen; 10828010), and 10 μM Y-27632 (Selleck Chemicals, Houston, TX; S1049). On days 18 and 19, iPSC-CMs were selected for resistance to zeocin 20 μg/mL (Fisher; R25001). From day 20 onward, iPSC-CMs were refreshed with RPMI 1640 minus glucose supplemented with 1× B27 and 4 mM lactate every two or three days.

#### Cloning of vectors

The lentiviral backbone, pSin-EF2-IRES-Pur, was a gift from James Thomson (Addgene, Watertown, MA; plasmid #16579). The TNNT2 promoter and zeocin resistance gene were amplified from TroponinT-GCaMP5-Zeo, a gift from John Gearhart (Addgene; plasmid #46027). The "empty" vector was assembled with the pSin backbone, TNNT2 promoter, and zeocin resistance gene. Full-length dystrophin cDNA was synthesized by Twist Bioscience (South San Francisco, CA). To clone microDYS1 (ΔR2-R15/ΔR18-R22/ΔC), the first amplicon (N terminus, hinge 1, and spectrin-like repeat 1), the second amplicon (spectrin-like repeats 16–17), and the third amplicon (spectrin-like repeats 23–24, hinge 4, and the cysteine-rich domain) were derived from full-length dystrophin. To clone microDYS2 (ΔR3-R19/ΔR20-R21/ΔC), the first amplicon (N terminus, hinge 1, and spectrin-like repeats 1–2), the second amplicon (hinge 3), and the third amplicon (spectrin-like repeats 22–24, hinge 4, and the cysteine-rich domain) were derived from full-length dystrophin. To clone microDYS3 (ΔR4-R23/ΔC), the first amplicon (N terminus, hinge 1, spectrin-like repeats 1–3, and hinge 2) and the second amplicon (spectrin-like repeat 24, hinge 4, and the cysteine-rich domain) were derived from full-length dystrophin. To clone miniDYS (ΔH2-R19), the first amplicon (N terminus, hinge 1, and spectrin-like repeats 1–3) and the second amplicon (hinge 3, spectrin-like repeats 20–24, hinge 4, cysteine-rich domain, and the C terminus) were derived from full-length dystrophin. All vectors were cloned by Gibson assembly into the pSin vector. Complete vector sequences were validated by nanopore sequencing (Plasmidsaurus, Louisville, KY).

#### Lentivirus production

Lentivirus was produced in HEK293T cells with a second-generation lentiviral system. The transfer plasmid, psPAX2 packaging plasmid, and pMD2.G envelope plasmid were transfected with Lipofectamine 2000 (Invitrogen; 11668500). Media containing virus were harvested 48–72 h post-transfection. Lentivirus was concentrated using Lenti-X Concentrator (Takara Bio, San Jose, CA; 631231), using the manufacturer's protocol. Transfer plasmid details are provided in Table S8.

#### Calcium imaging

For calcium imaging, iPSC-CMs were collected with Accutase:TrypLE on day 27 of differentiation. Glass-bottomed plates were micropatterned using Matrigel-coated PDMS stamps. iPSC-CMs were seeded at a density of 37,500 cells in 150 μL of RPMI 1640 minus glucose supplemented with 1X B27, 4 mM lactate, 5% KSR, and 10 μM Y-27632. After 30 min, 2 mL of RPMI 1640 minus glucose supplemented with 1X B27, 4 mM lactate, 5% KSR, and 10 μM Y-27632 was added to the well of the glass-bottomed plate. The cells were refreshed with RPMI 1640 minus glucose supplemented with 1X B27 and 4 mM lactate 2 days later and were imaged on day 30 of differentiation. To image, the cells were incubated with 4 μM Fura Red AM (Invitrogen; F3021) and 0.04% Pluronic F-127 (Invitrogen; P3000MP) at 37°C for 20 min. The cells were then washed with 2 mL PBS and refreshed with 3 mL RPMI 1640 without phenol red and glucose supplemented with 1X B27 and 4 mM lactate. The cells were incubated at 37°C for 15 min to allow for esterification of the AM dye. The cells were paced at 1 Hz and 20 V with a C-Pace EM (IonOptix, Westwood, MA) and captured at excitation wavelengths of 471 and 435 nm and emission wavelengths of 670 and 660 nm for 14 s. Videos were analyzed using a custom MATLAB script.

#### Viability assay

For viability assays, iPSC-CMs were collected with Accutase: TrypLE on day 27 of differentiation to be seeded into Matrigel-coated plates. iPSC-CMs were seeded in technical triplicate at a density of 24,000 cells per well of a 384-well plate (surface area of 0.084 $cm^2$). iPSC-CMs were seeded in RPMI 1640 minus glucose supplemented with 1X B27, 4 mM lactate, 5% KSR, and 10 μM Y-27632. The medium was replaced with RPMI 1640 minus glucose supplemented with 1X B27 and 4 mM lactate the next day. To measure viability, the cells were incubated with 20 nM TMRM (Invitrogen; T668) for 30 min at 37°C. After dye uptake, the cells were imaged with RPMI 1640 without phenol red and glucose supplemented with 1X B27 and 4 mM lactate. Entire wells were captured by taking 12 images of the well with a Keyence 10X objective. To track viability changes over time in the same wells, entire wells were imaged on day 30 of differentiation, refreshed with RPMI 1640 minus glucose supplemented with 1X B27 and 4 mM lactate every 2 days, and the same wells were imaged again on day 38 of differentiation. These images were stitched to create an image of the entire well. Percentages of viable cells were calculated by dividing TMRM-positive area on day 38 by the TMRM-positive area on day 30 in the same well. Percentages of viable cells across technical triplicates were averaged to obtain a single viability measurement per condition.

### Immunocytochemistry

For immunocytochemistry, iPSC-CMs were collected on day 27 of differentiation and seeded onto glass slides coated with Matrigel using Accutase:TrypLE into RPMI 1640 minus glucose supplemented with 1× B27, 4 mM lactate, 5% KSR, and 10 μM Y-27632. iPSC-CMs were refreshed with Accutase:TrypLE into RPMI 1640 minus glucose supplemented with 1× B27 and 4 mM lactate. On day 30 of differentiation, iPSC-CMs were fixed using 4% paraformaldehyde for 15 min. The cells were blocked and permeabilized in buffer containing 1% w/v BSA (Sigma Aldrich; A9647) and 0.1% Triton X-100 (Sigma-Aldrich; X100) in PBS for 1 h at room temperature. The cells were incubated with primary antibodies for cardiac troponin T (6.7 μg/mL, Abcam, Waltham, MA; ab45932), OCT4 (10 μg/mL, Millipore, Burlington, MA; MAB4419), SOX2 (120 ng/mL, Cell Signaling, Danvers, MA; 3579S), TRA-1-60 (114 ng/mL, Cell Signaling; 4746S), or NANOG (110 ng/mL, Cell Signaling; 4903S) overnight at 4°C. Then, the cells were washed 3 × 5 min in PBS. The cells incubated with antibodies for cardiac troponin T, OCT4, or TRA-1-60 were incubated with 4 μg/mL goat-anti mouse IgG secondary antibody (Abcam; ab150113). The cells incubated with antibodies for SOX2 or NANOG were incubated with 4 μg/mL goat-anti mouse IgG secondary antibody (Abcam; ab150115). Secondary incubations were done for 1 h at room temperature, then the cells were washed for 5 min in PBS. The cells were incubated with 300 nM DAPI (Invitrogen; D1306) for 15 min and then washed again for 5 min in PBS. Coverslips were mounted with Fluoromount-G (Southern Biotech, Birmingham, AL; 0100-01). Images were acquired on a Keyence or Zeiss microscope. Size and fluorescence intensities were analyzed using ImageJ.

### Bulk RNA-seq

For RNA-seq, iPSC-CMs were collected with Accutase:TrypLE on day 30 of differentiation and flash frozen. RNA was isolated from cells with the RNeasy Micro Kit (Qiagen, Germantown, MD 74104) using the manufacturer's protocol. Total RNA was sent to Novogene for quality control and bulk RNA-seq with poly(A) mRNA selection. To construct a pileup of the bulk RNA-seq data, sequencing reads were aligned to human GRCh38.p14 using STAR[65] (version 2.7.11b) and converted to aligned BAM files. BAM files were then converted to Bigwig files by using deepTools[66] (version 3.5.6). Bigwig files of the same condition were averaged using deepTools and UCSC Kent Utilities[67,68] (version 482). Averaged Bigwig files were then imported into IGV[69] (version 2.16.0) for visualization. For downstream analysis, sequencing reads were quasi-mapped, then counted to human GRCh38.p14 using Salmon[70] (version 1.8.0) with default settings for gene- and transcript-level quantifications. Salmon results were read into R, using the package tximport.[71] Quantification of dystrophin expression was performed by the transcripts per million (TPM) of the dystrophin gene inclusive of all transcripts that aligned with the gene. Differential gene expression analysis was performed on raw counts, using the R package DESeq2.[72] Genes and transcripts with more than 100 raw counts were considered as expressed. PCA and hierarchical clustering were performed based on transcript-specific quantification. Variance-stabilization transformed data from DESeq2 were used as the input for PCA and hierarchical clustering. The results from DESeq2 were estimated for effect size via Bayesian shrinkage estimators, using the R package lfcShrink.[73] To define DEGs, cutoff values of absolute $\log_2$ fold change greater than 1 and adjusted $p$ value less than 0.05 were used. DEGs were determined with reference to DMD empty CMs. $Z$ scores were used to generate heatmaps, using the R package Complex Heatmap.[74] GO enrichment analysis was performed using the R package ClusterProfiler.[75] All graphs were generated using the R package ggplot2.[76]

### RT-qPCR

For RT-qPCR, iPSC-CMs were collected with Accutase:TrypLE on day 30 of differentiation and flash frozen. RNA was isolated from cells with the RNeasy Micro Kit (Qiagen; 74104) using the manufacturer's protocol. RNA was reverse transcribed to cDNA with SuperScript IV Reverse Transcriptase (Invitrogen; 18090050), using 2.5 μM oligo $(dT)_{20}$, 2.5 μM random hexamers, and 500 μM dNTPs. mRNA expression levels were measured on a Quant Studio 6 Flex Real Time Detection System, using SsoAdvanced Universal SYBR Green Supermix (Bio Rad, Hercules, CA; 1725274) with 250 nM primers and 12.5 ng of cDNA. Primers specific to the dystrophin N terminus (DMD N terminus), hinge 1-spectrin-like repeat 1 (DMD H1-R1), spectrin repeats 16–17 (DMD R16–R17), and hinge 4 (DMD H4) were used to quantify dystrophin mRNA expression. Data were analyzed using ΔΔCT and normalized to GAPDH. Relative fold change of mRNA was normalized to DMD empty iPSC-CMs. Primer sequences are provided in Table S9.

### Western blotting

Cells were flash frozen and lysed in lysis buffer (50 mM Tris-HCl, pH 7.5; 150 mM NaCl; 1% Triton X-100; and 0.1% sodium deoxycholate). 80 μg of total protein was loaded on a 7.5% Tris-glycine-SDS polyacrylamide gel, using 1× Laemmli sample buffer (Bio-Rad; 1610747) and β-mercaptoethanol (2.5% final concentration). The gel was run in 25 mM Tris, 192 mM glycine, and 0.1% SDS (pH 8.3) for 10 min at 85 V then 2 h at 140 V. A wet transfer to 0.45 μm nitrocellulose membrane was done using Towbin buffer with 10% methanol at 90 V for 1.5 h at 4°C. The membrane was blocked in 5% BSA for 1 h and then incubated overnight at 4°C with the following primary antibodies: 2 μg/mL MANHINGE4B (DSHB, Iowa City, IA), 2 μg/mL C-terminal dystrophin antibody (Abcam; ab15277), and 850 ng/mL sarcomeric alpha actinin (Sigma-Aldrich; A7732). For secondary antibodies, the blots were incubated with goat anti mouse IgG1-HRP at 1:2,500 (Invitrogen; A10551) or goat-anti rabbit IgG-HRP at 1:10,000 (Abcam; ab97051) for 1 h at room temperature. Between incubations, the membrane was washed 3 × 10 min in Tris-buffered saline with 0.1% Tween 20. The membrane was imaged by chemiluminescence (Nacalai Tesque, San Diego, CA; 07880) on a Bio-Rad ChemiDoc MP System.

### Statistical analysis

Statistical analyses were performed using GraphPad Prism 10.5, SPSS Statistics 30.0, and RStudio 4.5. (2025.05.0 + 496). Outliers were identified using the robust regression and outlier removal test (ROUT), with Q = 1% false discovery rate. For analyses involving one variable across multiple groups, one-way ANOVA with Kruskal-Wallis test for multiple comparison was used for all data that were non-parametric, with the null hypothesis assuming that all group medians are equal. Categorical data were analyzed using Pearson's chi-squared test with 5 degrees of freedom. Power analyses were performed using G*Power[77] (version 3.1.9.6). The Wilcoxon-Mann-Whitney test ($\alpha = 0.05$) was used, assuming non-parametric distributions with minimum asymptotic relative efficiency (Table S7). Data are represented as medians with IQRs, and statistical significance was defined as $p < 0.05$.

## DATA AND CODE AVAILABILITY

All data supporting the findings of this study are available in the primary figures and the supplemental material. Materials, including lentiviral vectors, will be made available on reasonable request and following execution of a material(s) transfer agreement. RNA-seq data are available from the GEO accession number GEO: GSE310327.

## ACKNOWLEDGMENTS

The authors thank the Sue and Bill Gross Stem Cell Research Center Core Facility for their support as well as David L. Mack, PhD, and Chris Denning, PhD, for the human iPSC lines. This study was supported by grants from the National Institutes of Health (K01HL169413 to A.E.), the American Heart Association (https://doi.org/10.58275/AHA.24CDA1259424.pc.gr.193591) to A.E., the Muscular Dystrophy Association (https://doi.org/10.55762/pc.gr.157032) to A.E., UCI School of Medicine New Investigator Faculty Research Grant to A.E., T32 Predoctoral Training Fellowship (T32AR083870) to A.R.K., the California Institute of Regenerative Medicine Bridges Program (EDUC2-12734) to J.H.L., and the Summer Undergraduate Research Program Fellowship to H.D.

## AUTHOR CONTRIBUTIONS

A.E. conceived the project; A.R.K. and A.E designed the experiments; A.R.K., A.F.G.S.G., R.Z, H.D., F.L., E.C.L., L.C.M., S.B., A.M., M.K.P., D.S.O., J.H.L., and A.E. performed the experiments, collected the data, and analyzed the results; S.I.T.-B. analyzed the results; A.R.K. and A.E. contributed to the analysis and interpretation; A.R.K. and A.E. wrote the manuscript; A.E. oversaw all aspects of this work; A.E. and A.R.K. wrote the grant applications that funded this project.

## DECLARATION OF INTERESTS

The authors declare no competing interests.

## SUPPLEMENTAL INFORMATION

Supplemental information can be found online at https://doi.org/10.1016/j.omta.2026.201801.

## REFERENCES

1. Crisafulli, S., Sultana, J., Fontana, A., Salvo, F., Messina, S., and Trifirò, G. (2020). Global epidemiology of Duchenne muscular dystrophy: an updated systematic review and meta-analysis. Orphanet J. Rare Dis. *15*, 141. https://doi.org/10.1186/s13023-020-01430-8.

2. Duan, D., Goemans, N., Takeda, S., Mercuri, E., and Aartsma-Rus, A. (2021). Duchenne muscular dystrophy. Nat. Rev. Dis. Primers *7*, 13–19. https://doi.org/10.1038/s41572-021-00248-3.

3. Connuck, D.M., Sleeper, L.A., Colan, S.D., Cox, G.F., Towbin, J.A., Lowe, A.M., Wilkinson, J.D., Orav, E.J., Cuniberti, L., Salbert, B.A., et al. (2008). Characteristics and outcomes of cardiomyopathy in children with Duchenne or Becker muscular dystrophy: A comparative study from the Pediatric Cardiomyopathy Registry. Am. Heart J. *155*, 998–1005. https://doi.org/10.1016/j.ahj.2008.01.018.

4. Yilmaz, A., Gdynia, H.-J., Baccouche, H., Mahrholdt, H., Meinhardt, G., Basso, C., Thiene, G., Sperfeld, A.-D., Ludolph, A.C., and Sechtem, U. (2008). Cardiac involvement in patients with Becker muscular dystrophy: new diagnostic and pathophysiological insights by a CMR approach. J. Cardiovasc. Magn. Reson. *10*, 50. https://doi.org/10.1186/1532-429X-10-50.

5. Hoffman, E.P., Fischbeck, K.H., Brown, R.H., Johnson, M., Medori, R., Loike, J.D., Harris, J.B., Waterston, R., Brooke, M., Specht, L., et al. (1988). Characterization of Dystrophin in Muscle-Biopsy Specimens from Patients with Duchenne's or Becker's Muscular Dystrophy. N. Engl. J. Med. *318*, 1363–1368. https://doi.org/10.1056/NEJM198805263182104.

6. Hoffman, E.P., Brown, R.H., and Kunkel, L.M. (1987). Dystrophin: The protein product of the duchenne muscular dystrophy locus. Cell *51*, 919–928. https://doi.org/10.1016/0092-8674(87)90579-4.

7. Ohlendieck, K., Matsumura, K., Ionasescu, V.V., Towbin, J.A., Bosch, E.P., Weinstein, S.L., Sernett, S.W., and Campbell, K.P. (1993). Duchenne muscular dystrophy: Deficiency of dystrophin-associated proteins in the sarcolemma. Neurology *43*, 795–800. https://doi.org/10.1212/WNL.43.4.795.

8. Koenig, M., Monaco, A.P., and Kunkel, L.M. (1988). The complete sequence of dystrophin predicts a rod-shaped cytoskeletal protein. Cell *53*, 219–228. https://doi.org/10.1016/0092-8674(88)90383-2.

9. Hammonds, R.G. (1987). Protein sequence of DMD gene is related to actin-binding domain of α-actinin. Cell *51*, 1. https://doi.org/10.1016/0092-8674(87)90002-X.

10. Kaspar, R.W., Allen, H.D., Ray, W.C., Alvarez, C.E., Kissel, J.T., Pestronk, A., Weiss, R.B., Flanigan, K.M., Mendell, J.R., and Montanaro, F. (2009). Analysis of dystrophin deletion mutations predicts age of cardiomyopathy onset in becker muscular dystrophy. Circ. Cardiovasc. Genet. *2*, 544–551. https://doi.org/10.1161/CIRCGENETICS.109.867242.

11. Le, S., Yu, M., Hovan, L., Zhao, Z., Ervasti, J., and Yan, J. (2018). Dystrophin As a Molecular Shock Absorber. ACS Nano *12*, 12140–12148. https://doi.org/10.1021/acsnano.8b05721.

12. Jung, D., Yang, B., Meyer, J., Chamberlain, J.S., and Campbell, K.P. (1995). Identification and Characterization of the Dystrophin Anchoring Site on β-Dystroglycan. J. Biol. Chem. *270*, 27305–27310. https://doi.org/10.1074/jbc.270.45.27305.

13. Sadoulet-Puccio, H.M., Rajala, M., and Kunkel, L.M. (1997). Dystrobrevin and dystrophin: An interaction through coiled-coil motifs. Proc. Natl. Acad. Sci. *94*, 12413–12418. https://doi.org/10.1073/pnas.94.23.12413.

14. Kamdar, F., and Garry, D.J. (2016). Dystrophin-Deficient Cardiomyopathy. J. Am. Coll. Cardiol. *67*, 2533–2546. https://doi.org/10.1016/j.jacc.2016.02.081.

15. McDonald, C.M., Henricson, E.K., Abresch, R.T., Duong, T., Joyce, N.C., Hu, F., Clemens, P.R., Hoffman, E.P., Cnaan, A., and Gordish-Dressman, H.; CINRG Investigators (2018). Long-term effects of glucocorticoids on function, quality of life, and survival in patients with Duchenne muscular dystrophy: a prospective cohort study. Lancet *391*, 451–461. https://doi.org/10.1016/S0140-6736(17)32160-8.

16. DeSilva, S., Drachman, D.B., Mellits, D., and Kuncl, R.W. (1987). Prednisone Treatment in Duchenne Muscular Dystrophy: Long-term Benefit. Arch. Neurol. *44*, 818–822. https://doi.org/10.1001/archneur.1987.00520200022012.

17. Wilton, S.D., Fall, A.M., Harding, P.L., McClorey, G., Coleman, C., and Fletcher, S. (2007). Antisense Oligonucleotide-induced Exon Skipping Across the Human Dystrophin Gene Transcript. Mol. Ther. *15*, 1288–1296. https://doi.org/10.1038/sj.mt.6300095.

18. Frank, D.E., Schnell, F.J., Akana, C., El-Husayni, S.H., Desjardins, C.A., Morgan, J., Charleston, J.S., Sardone, V., Domingos, J., Dickson, G., et al. (2020). Increased dystrophin production with golodirsen in patients with Duchenne muscular dystrophy. Neurology *94*, e2270–e2282. https://doi.org/10.1212/WNL.0000000000009233.

19. Clemens, P.R., Rao, V.K., Connolly, A.M., Harper, A.D., Mah, J.K., Smith, E.C., McDonald, C.M., Zaidman, C.M., Morgenroth, L.P., Osaki, H., et al. (2020). Safety, Tolerability, and Efficacy of Viltolarsen in Boys With Duchenne Muscular Dystrophy Amenable to Exon 53 Skipping: A Phase 2 Randomized Clinical Trial. JAMA Neurol. *77*, 982–991. https://doi.org/10.1001/jamaneurol.2020.1264.

20. McDonald, C.M., Shieh, P.B., Abdel-Hamid, H.Z., Connolly, A.M., Ciafaloni, E., Wagner, K.R., Goemans, N., Mercuri, E., Khan, N., Koenig, E., et al. (2021). Open-Label Evaluation of Eteplirsen in Patients with Duchenne Muscular Dystrophy Amenable to Exon 51 Skipping: PROMOVI Trial. J. Neuromuscul. Dis. *8*, 989–1001. https://doi.org/10.3233/JND-210643.

21. Vasterling, M.E., Maitski, R.J., Davis, B.A., Barnes, J.E., Kelkar, R.A., Klapper, R.J., Patel, H., Ahmadzadeh, S., Shekoohi, S., Kaye, A.D., and Varrassi, G. (2023). AMONDYS 45 (Casimersen), a Novel Antisense Phosphorodiamidate Morpholino Oligomer: Clinical Considerations for Treatment in Duchenne Muscular Dystrophy. Cureus *15*, e51237. https://doi.org/10.7759/cureus.51237.

22. Arcudi, A., Di Francesco, M., Rodolico, D., and D'Amario, D. (2022). Angiotensin receptor-neprilysin inhibitor in symptomatic patients with Duchenne dilated cardiomyopathy: A primetime. ESC Heart Fail. *9*, 3639–3642. https://doi.org/10.1002/ehf2.13963.

23. Bostick, B., Yue, Y., Long, C., and Duan, D. (2008). Prevention of Dystrophin-Deficient Cardiomyopathy in Twenty-One-Month-Old Carrier Mice by Mosaic Dystrophin Expression or Complementary Dystrophin/Utrophin Expression. Circ. Res. *102*, 121–130. https://doi.org/10.1161/CIRCRESAHA.107.162982.

24. Eguchi, A., Gonzalez, A.F.G.S., Torres-Bigio, S.I., Koleckar, K., Birnbaum, F., Zhang, J.Z., Wang, V.Y., Wu, J.C., Artandi, S.E., and Blau, H.M. (2023). TRF2 rescues telomere attrition and prolongs cell survival in Duchenne muscular dystrophy cardiomyocytes derived from human iPSCs. Proc. Natl. Acad. Sci. USA *120*, e2209967120. https://doi.org/10.1073/pnas.2209967120.

25. Chang, A.C.Y., Pardon, G., Chang, A.C.H., Wu, H., Ong, S.-G., Eguchi, A., Ancel, S., Holbrook, C., Ramunas, J., Ribeiro, A.J.S., et al. (2021). Increased tissue stiffness triggers contractile dysfunction and telomere shortening in dystrophic cardiomyocytes. Stem Cell Rep. *16*, 2169–2181. https://doi.org/10.1016/j.stemcr.2021.04.018.

26. Dong, J.-Y., Fan, P.-D., and Frizzell, R.A. (1996). Quantitative Analysis of the Packaging Capacity of Recombinant Adeno-Associated Virus. Hum. Gene Ther. *7*, 2101–2112. https://doi.org/10.1089/hum.1996.7.17-2101.

27. Chwalenia, K., Feng, V.-Y., Hemmer, N., Friedrichsen, H.J., Vorobieva, I., Wood, M.J.A., and Roberts, T.C. (2025). AAV microdystrophin gene replacement therapy for Duchenne muscular dystrophy: progress and prospects. Gene Ther. *32*, 447–461. https://doi.org/10.1038/s41434-025-00561-6.

28. Wang, B., Li, J., and Xiao, X. (2000). Adeno-associated virus vector carrying human minidystrophin genes effectively ameliorates muscular dystrophy in *mdx* mouse model. Proc. Natl. Acad. Sci. *97*, 13714–13719. https://doi.org/10.1073/pnas.240335297.

29. Harper, S.Q., Hauser, M.A., DelloRusso, C., Duan, D., Crawford, R.W., Phelps, S.F., Harper, H.A., Robinson, A.S., Engelhardt, J.F., Brooks, S.V., and Chamberlain, J.S. (2002). Modular flexibility of dystrophin: Implications for gene therapy of Duchenne muscular dystrophy. Nat. Med. *8*, 253–261. https://doi.org/10.1038/nm0302-253.

30. Hakim, C.H., Wasala, N.B., Pan, X., Kodippili, K., Yue, Y., Zhang, K., Yao, G., Haffner, B., Duan, S.X., Ramos, J., et al. (2017). A Five-Repeat Micro-Dystrophin Gene Ameliorated Dystrophic Phenotype in the Severe DBA/2J-mdx Model of Duchenne Muscular Dystrophy. Mol. Ther. Methods Clin. Dev. *6*, 216–230. https://doi.org/10.1016/j.omtm.2017.06.006.

31. Foltz, S.J., Qian, R., Yang, J., Elliott, K., Heithoff, B.P., Jasick, H., Smith, J.B., Karumuthil-Melethil, S., Qiao, C., Liu, Y., and Danos, O. (2025). Enhanced therapeutic potential of a microdystrophin with an extended C-terminal domain. Mol. Ther. Methods Clin. Dev. *33*, 101519. https://doi.org/10.1016/j.omtm.2025.101519.

32. Bostick, B., Shin, J.-H., Yue, Y., and Duan, D. (2011). AAV-microdystrophin Therapy Improves Cardiac Performance in Aged Female mdx Mice. Mol. Ther. *19*, 1826–1832. https://doi.org/10.1038/mt.2011.154.

33. Townsend, D., Blankinship, M.J., Allen, J.M., Gregorevic, P., Chamberlain, J.S., and Metzger, J.M. (2007). Systemic Administration of Micro-dystrophin Restores Cardiac Geometry and Prevents Dobutamine-induced Cardiac Pump Failure. Mol. Ther. *15*, 1086–1092. https://doi.org/10.1038/sj.mt.6300144.

34. England, S.B., Nicholson, L.V., Johnson, M.A., Forrest, S.M., Love, D.R., Zubrzycka-Gaarn, E.E., Bulman, D.E., Harris, J.B., and Davies, K.E. (1990). Very mild muscular dystrophy associated with the deletion of 46% of dystrophin. Nature *343*, 180–182. https://doi.org/10.1038/343180a0.

35. Davies, K.E., and Vogt, J. (2024). Long-term clinical follow-up of a family with Becker muscular dystrophy associated with a large deletion in the DMD gene. Neuromuscul. Disord. *39*, 5–9. https://doi.org/10.1016/j.nmd.2024.04.004.

36. Dick, E., Matsa, E., Bispham, J., Reza, M., Guglieri, M., Staniforth, A., Watson, S., Kumari, R., Lochmüller, H., Young, L., et al. (2011). Two new protocols to enhance the production and isolation of human induced pluripotent stem cell lines. Stem Cell Res. *6*, 158–167. https://doi.org/10.1016/j.scr.2010.10.002.

37. Dick, E., Kalra, S., Anderson, D., George, V., Ritso, M., Laval, S.H., Barresi, R., Aartsma-Rus, A., Lochmüller, H., and Denning, C. (2013). Exon Skipping and Gene Transfer Restore Dystrophin Expression in Human Induced Pluripotent Stem Cells-Cardiomyocytes Harboring *DMD* Mutations. Stem Cell. Dev. *22*, 2714–2724. https://doi.org/10.1089/scd.2013.0135.

38. Guan, X., Mack, D.L., Moreno, C.M., Strande, J.L., Mathieu, J., Shi, Y., Markert, C.D., Wang, Z., Liu, G., Lawlor, M.W., et al. (2014). Dystrophin-deficient cardiomyocytes derived from human urine: New biologic reagents for drug discovery. Stem Cell Res. *12*, 467–480. https://doi.org/10.1016/j.scr.2013.12.004.

39. Pioner, J.M., Guan, X., Klaiman, J.M., Racca, A.W., Pabon, L., Muskheli, V., Macadangdang, J., Ferrantini, C., Hoopmann, M.R., Moritz, R.L., et al. (2020). Absence of full-length dystrophin impairs normal maturation and contraction of cardiomyocytes derived from human-induced pluripotent stem cells. Cardiovasc. Res. *116*, 368–382. https://doi.org/10.1093/cvr/cvz109.

40. Lai, Y., Thomas, G.D., Yue, Y., Yang, H.T., Li, D., Long, C., Judge, L., Bostick, B., Chamberlain, J.S., Terjung, R.L., and Duan, D. (2009). Dystrophins carrying spectrin-like repeats 16 and 17 anchor nNOS to the sarcolemma and enhance exercise performance in a mouse model of muscular dystrophy. J. Clin. Investig. *119*, 624–635. https://doi.org/10.1172/JCI36612.

41. Prins, K.W., Humston, J.L., Mehta, A., Tate, V., Ralston, E., and Ervasti, J.M. (2009). Dystrophin is a microtubule-associated protein. J. Cell Biol. *186*, 363–369. https://doi.org/10.1083/jcb.200905048.

42. Zhao, J., Kodippili, K., Yue, Y., Hakim, C.H., Wasala, L., Pan, X., Zhang, K., Yang, N.N., Duan, D., and Lai, Y. (2016). Dystrophin contains multiple independent membrane-binding domains. Hum. Mol. Genet. *25*, 3647–3653. https://doi.org/10.1093/hmg/ddw210.

43. Addis, R.C., Ifkovits, J.L., Pinto, F., Kellam, L.D., Esteso, P., Rentschler, S., Christoforou, N., Epstein, J.A., and Gearhart, J.D. (2013). Optimization of direct fibroblast reprogramming to cardiomyocytes using calcium activity as a functional measure of success. J. Mol. Cell. Cardiol. *60*, 97–106. https://doi.org/10.1016/j.yjmcc.2013.04.004.

44. Lian, X., Hsiao, C., Wilson, G., Zhu, K., Hazeltine, L.B., Azarin, S.M., Raval, K.K., Zhang, J., Kamp, T.J., and Palecek, S.P. (2012). Robust cardiomyocyte differentiation from human pluripotent stem cells via temporal modulation of canonical Wnt signaling. Proc. Natl. Acad. Sci. USA *109*, E1848–E1857. https://doi.org/10.1073/pnas.1200250109.

45. Wakai, S., Minami, R., Kameda, K., Okabe, M., Nagaoka, M., Annaka, S., Higashidate, Y., Tomita, H., and Tachi, N. (1988). Electron microscopic study of the biopsied cardiac muscle in Duchenne muscular dystrophy. J. Neurol. Sci. *84*, 167–175. https://doi.org/10.1016/0022-510X(88)90122-0.

46. Atmanli, A., Chai, A.C., Cui, M., Wang, Z., Nishiyama, T., Bassel-Duby, R., and Olson, E.N. (2021). Cardiac Myoediting Attenuates Cardiac Abnormalities in Human and Mouse Models of Duchenne Muscular Dystrophy. Circ. Res. *129*, 602–616. https://doi.org/10.1161/CIRCRESAHA.121.319579.

47. Kamdar, F., Das, S., Gong, W., Klaassen Kamdar, A., Meyers, T.A., Shah, P., Ervasti, J.M., Townsend, D., Kamp, T.J., Wu, J.C., et al. (2020). Stem Cell–Derived Cardiomyocytes and Beta-Adrenergic Receptor Blockade in Duchenne Muscular Dystrophy Cardiomyopathy. J. Am. Coll. Cardiol. *75*, 1159–1174. https://doi.org/10.1016/j.jacc.2019.12.066.

48. Kyrychenko, V., Kyrychenko, S., Tiburcy, M., Shelton, J.M., Long, C., Schneider, J.W., Zimmermann, W.-H., Bassel-Duby, R., and Olson, E.N. (2017). Functional correction of dystrophin actin binding domain mutations by genome editing. JCI Insight *2*, e95918. https://doi.org/10.1172/jci.insight.95918.

49. Pioner, J.M., Santini, L., Palandri, C., Langione, M., Grandinetti, B., Querceto, S., Martella, D., Mazzantini, C., Scellini, B., Giammarino, L., et al. (2022). Calcium handling maturation and adaptation to increased substrate stiffness in human

iPSC-derived cardiomyocytes: The impact of full-length dystrophin deficiency. Front. Physiol. *13*, 1030920. https://doi.org/10.3389/fphys.2022.1030920.

50. Birnbaum, F., Eguchi, A., Pardon, G., Chang, A.C.Y., and Blau, H.M. (2022). Tamoxifen treatment ameliorates contractile dysfunction of Duchenne muscular dystrophy stem cell-derived cardiomyocytes on bioengineered substrates. npj Regen. Med. *7*, 19. https://doi.org/10.1038/s41536-022-00214-x.

51. Paik, D.T., Chandy, M., and Wu, J.C. (2020). Patient and Disease–Specific Induced Pluripotent Stem Cells for Discovery of Personalized Cardiovascular Drugs and Therapeutics. Pharmacol. Rev. *72*, 320–342. https://doi.org/10.1124/pr.116.013003.

52. Tohyama, S., Hattori, F., Sano, M., Hishiki, T., Nagahata, Y., Matsuura, T., Hashimoto, H., Suzuki, T., Yamashita, H., Satoh, Y., et al. (2013). Distinct metabolic flow enables large-scale purification of mouse and human pluripotent stem cell-derived cardiomyocytes. Cell Stem Cell *12*, 127–137. https://doi.org/10.1016/j.stem.2012.09.013.

53. Tasfaout, H., Halbert, C.L., McMillen, T.S., Allen, J.M., Reyes, T.R., Flint, G.V., Grimm, D., Hauschka, S.D., Regnier, M., and Chamberlain, J.S. (2024). Split intein-mediated protein trans-splicing to express large dystrophins. Nature *632*, 192–200. https://doi.org/10.1038/s41586-024-07710-8.

54. Zhou, Y., Zhang, C., Xiao, W., Herzog, R.W., and Han, R. (2024). Systemic delivery of full-length dystrophin in Duchenne muscular dystrophy mice. Nat. Commun. *15*, 6141. https://doi.org/10.1038/s41467-024-50569-6.

55. Tasfaout, H., McMillen, T.S., Reyes, T.R., Halbert, C.L., Tian, R., Regnier, M., and Chamberlain, J.S. (2025). Expression of full-length dystrophin reverses muscular dystrophy defects in young and old mdx4cv mice. J. Clin. Investig. *135*, e189075. https://doi.org/10.1172/jci189075.

56. Chamberlain, J.S., Metzger, J., Reyes, M., Townsend, D., and Faulkner, J.A. (2007). Dystrophin-deficient *mdx* mice display a reduced life span and are susceptible to spontaneous rhabdomyosarcoma. FASEB J. *21*, 2195–2204. https://doi.org/10.1096/fj.06-7353com.

57. Bostick, B., Yue, Y., and Duan, D. (2010). Gender influences cardiac function in the *mdx* model of duchenne cardiomyopathy. Muscle Nerve *42*, 600–603. https://doi.org/10.1002/mus.21763.

58. Forand, A., Moog, S., Mougenot, N., Lemaitre, M., Sevoz-Couche, C., Guesmia, Z., Virtanen, L., Giordani, L., Muchir, A., and Pietri-Rouxel, F. (2025). Long-Term Dystrophin Replacement Therapy in Duchenne Muscular Dystrophy Causes Cardiac Inflammation. JACC, Basic Transl. Sci. *10*, 759–782. https://doi.org/10.1016/j.jacbts.2024.12.015.

59. Hart, C.C., Lee, Y.I., Xie, J., Gao, G., Lin, B.L., Hammers, D.W., and Sweeney, H.L. (2024). Potential limitations of microdystrophin gene therapy for Duchenne muscular dystrophy. JCI Insight *9*, e165869. https://doi.org/10.1172/jci.insight.165869.

60. Banks, G.B., Judge, L.M., Allen, J.M., and Chamberlain, J.S. (2010). The Polyproline Site in Hinge 2 Influences the Functional Capacity of Truncated Dystrophins. PLoS Genet. *6*, e1000958. https://doi.org/10.1371/journal.pgen.1000958.

61. Howard, Z.M., Dorn, L.E., Lowe, J., Gertzen, M.D., Ciccone, P., Rastogi, N., Odom, G.L., Accornero, F., Chamberlain, J.S., and Rafael-Fortney, J.A. (2021). Micro-dystrophin gene therapy prevents heart failure in an improved Duchenne muscular dystrophy cardiomyopathy mouse model. JCI Insight *6*, e146511. https://doi.org/10.1172/jci.insight.146511.

62. Butterfield, R.J., Shieh, P.B., Li, H., Binks, M., McDonnell, T.G., Ryan, K.A., Delnomdedieu, M., Belluscio, B.A., Neelakantan, S., Levy, D.I., et al. (2025). AAV mini-dystrophin gene therapy for Duchenne muscular dystrophy: a phase 1b trial. Nat. Med. *31*, 2712–2721. https://doi.org/10.1038/s41591-025-03750-3.

63. Mendell, J.R., Sahenk, Z., Lehman, K., Nease, C., Lowes, L.P., Miller, N.F., Iammarino, M.A., Alfano, L.N., Nicholl, A., Al-Zaidy, S., et al. (2020). Assessment of Systemic Delivery of rAAVrh74.MHCK7.micro-dystrophin in Children With Duchenne Muscular Dystrophy: A Nonrandomized Controlled Trial. JAMA Neurol. *77*, 1122–1131. https://doi.org/10.1001/jamaneurol.2020.1484.

64. Mendell, J.R., Muntoni, F., McDonald, C.M., Mercuri, E.M., Ciafaloni, E., Komaki, H., Leon-Astudillo, C., Nascimento, A., Proud, C., Schara-Schmidt, U., et al. (2025). AAV gene therapy for Duchenne muscular dystrophy: the EMBARK phase 3 randomized trial. Nat. Med. *31*, 332–341. https://doi.org/10.1038/s41591-024-03304-z.

65. Dobin, A., Davis, C.A., Schlesinger, F., Drenkow, J., Zaleski, C., Jha, S., Batut, P., Chaisson, M., and Gingeras, T.R. (2013). STAR: ultrafast universal RNA-seq aligner. Bioinformatics *29*, 15–21. https://doi.org/10.1093/bioinformatics/bts635.

66. Ramírez, F., Ryan, D.P., Grüning, B., Bhardwaj, V., Kilpert, F., Richter, A.S., Heyne, S., Dündar, F., and Manke, T. (2016). deepTools2: a next generation web server for deep-sequencing data analysis. Nucleic Acids Res. *44*, W160–W165. https://doi.org/10.1093/nar/gkw257.

67. Kent, W.J., Zweig, A.S., Barber, G., Hinrichs, A.S., and Karolchik, D. (2010). BigWig and BigBed: enabling browsing of large distributed datasets. Bioinformatics *26*, 2204–2207. https://doi.org/10.1093/bioinformatics/btq351.

68. Casper, J., Speir, M.L., Raney, B.J., Perez, G., Nassar, L.R., Lee, C.M., Hinrichs, A.S., Gonzalez, J.N., Fischer, C., Diekhans, M., et al. (2026). The UCSC Genome Browser database: 2026 update. Nucleic Acids Res. *54*, D1331–D1335. https://doi.org/10.1093/nar/gkaf1250.

69. Robinson, J.T., Thorvaldsdóttir, H., Winckler, W., Guttman, M., Lander, E.S., Getz, G., and Mesirov, J.P. (2011). Integrative genomics viewer. Nat. Biotechnol. *29*, 24–26. https://doi.org/10.1038/nbt.1754.

70. Patro, R., Duggal, G., Love, M.I., Irizarry, R.A., and Kingsford, C. (2017). Salmon provides fast and bias-aware quantification of transcript expression. Nat. Methods *14*, 417–419. https://doi.org/10.1038/nmeth.4197.

71. Soneson, C., Love, M.I., and Robinson, M.D. (2015). Differential analyses for RNA-seq: transcript-level estimates improve gene-level inferences. F1000Res. *4*, 1521. https://doi.org/10.12688/f1000research.7563.1.

72. Love, M.I., Huber, W., and Anders, S. (2014). Moderated estimation of fold change and dispersion for RNA-seq data with DESeq2. Genome Biol. *15*, 550. https://doi.org/10.1186/s13059-014-0550-8.

73. Zhu, A., Ibrahim, J.G., and Love, M.I. (2019). Heavy-tailed prior distributions for sequence count data: removing the noise and preserving large differences. Bioinformatics *35*, 2084–2092. https://doi.org/10.1093/bioinformatics/bty895.

74. Gu, Z., Eils, R., and Schlesner, M. (2016). Complex heatmaps reveal patterns and correlations in multidimensional genomic data. Bioinformatics *32*, 2847–2849. https://doi.org/10.1093/bioinformatics/btw313.

75. Yu, G., Wang, L.-G., Han, Y., and He, Q.-Y. (2012). clusterProfiler: an R Package for Comparing Biological Themes Among Gene Clusters. OMICS A J. Integr. Biol. *16*, 284–287. https://doi.org/10.1089/omi.2011.0118.

76. Wickham, H. (2016). ggplot2: Elegant Graphics for Data Analysis, 2nd ed. 2016 (Springer International Publishing : Imprint: Springer). https://doi.org/10.1007/978-3-319-24277-4.

77. Faul, F., Erdfelder, E., Lang, A.-G., and Buchner, A. (2007). G*Power 3: A flexible statistical power analysis program for the social, behavioral, and biomedical sciences. Behav. Res. Methods *39*, 175–191. https://doi.org/10.3758/BF03193146.

**OMTA, Volume *34***

## Supplemental information

# Microdystrophins partially rescue deficits of Duchenne muscular dystrophy iPSC-cardiomyocytes

**Abiageal R. Keegan, Adriana Fernanda G.S. Gonzalez, Rongruo Zhang, Hung Doan, Sofía I. Torres-Bigio, Fiona Lau, Kaulen N. Ly, Elaine C. Lai, Leahlyn C. Mamuyac, Sriram Bhimaraju, Abhishree Mishra, Michelle K. Polen, Daniel S. Ortiz, Jay H. Lam, and Asuka Eguchi**

**Supplemental Information**

**Table S1. Differentially expressed genes from pairwise comparisons**. The first five tabs of the spreadsheet contain differentially expressed genes compiled from pairwise comparisons between the condition (Control Empty, DMD microDYS1, DMD microDYS2, DMD microDYS3, DMD miniDYS) and DMD Empty iPSC-CMs. DMD Empty was considered the reference condition. The next four tabs of the spreadsheet contain differentially expressed genes compiled from pairwise comparisons between the condition (DMD microDYS1, DMD microDYS2, DMD microDYS3, DMD miniDYS) and Control Empty iPSC-CMs. Control Empty was considered the reference condition. Negative $\log_2$ fold change means downregulated in the condition with respect to reference. Positive $\log_2$ fold change means upregulated in the condition with respect to reference. DEGs were assessed with Transcript IDs. DEGs were defined with a cutoff value of absolute $\log_2$ fold change >1 and FDR <0.05.

**Table S2. Differentially expressed genes from bulk RNA-seq clustering.** The spreadsheet contains the differentially expressed genes in each cluster of Figure 3F.

**Table S3. Gene Ontology terms from clustering.** The spreadsheet contains Gene Ontology (GO) enrichment analysis results provided by the R package clusterProfiler compiled from the DEGs identified in each cluster of Figure 3F. DEGs were defined with cutoff values of absolute $\log_2$ fold change >1 and FDR <0.05. Ontology refers to which branch of the GO hierarchy the term belongs to (BP = biological process, CC = cellular component, MF = molecular function). GeneRatio is calculated by dividing the number of genes in the GO category divided by the number of DEGs. BgRatio refers to the ratio of reference genes that fall into the GO term. RichFactor is calculated by dividing the number of genes in the category by the expected count of genes belonging in the GO ID by chance. Fold enrichment is calculated by dividing the GeneRatio by BgRatio.

**Table S4. Gene Ontology terms.** The first five tabs of the spreadsheet contain Gene Ontology (GO) enrichment analysis results provided by the R package clusterProfiler compiled from the DEGs derived from pairwise comparisons between the sample (Control Empty, DMD microDYS1, DMD microDYS2, DMD microDYS3, DMD miniDYS) and DMD Empty iPSC-CMs. DMD Empty was considered the reference condition. The next four tabs of the spreadsheet contain GO enrichment analysis results compiled from the DEGs derived from pairwise comparisons between the sample (DMD microDYS1, DMD microDYS2, DMD microDYS3, and DMD miniDYS) and Control Empty iPSC-CMs. Control Empty was considered the reference condition. DEGs were defined with cutoff values of absolute $\log_2$ fold change >1 and FDR <0.05. Ontology refers to which branch of the GO hierarchy the term belongs to (BP = biological process, CC = cellular component, MF = molecular function). GeneRatio is calculated by dividing the number of genes in the GO category divided by the number of DEGs. BgRatio refers to the ratio of reference genes that fall into the GO term. RichFactor is calculated by dividing the number of genes in the category by the expected count of genes belonging in the GO ID by chance. Fold enrichment is calculated by dividing the GeneRatio by BgRatio.

**Table S5. p-values for chi-squared test**
Bonferroni corrected *p*-values for calcium data

| **Fig. 4B** DMD19 | **Arrhythmic** | | | | |
|---|---|---|---|---|---|
| | **Count** | **Total** | **% of Total** | **Adjusted Residual** | **Corrected p-value** |
| Control Empty | 11 | 47 | 23.4 | -3.627 | 0.002 |
| DMD Empty | 40 | 61 | 65.6 | 2.954 | 0.019 |
| DMD microDYS1 | 36 | 54 | 66.7 | 3.018 | 0.015 |
| DMD microDYS2 | 29 | 50 | 58.0 | 1.552 | 0.724 |
| DMD microDYS3 | 25 | 59 | 42.4 | -0.936 | > 0.999 |
| DMD miniDYS | 20 | 61 | 32.8 | -2.717 | 0.040 |
| **Fig. S12A** UC | **Arrhythmic** | | | | |
| | **Count** | **Total** | **% of Total** | **Adjusted Residual** | **Corrected p-value** |
| Control Empty | 13 | 62 | 21.0 | -3.585 | 0.002 |
| DMD Empty | 33 | 57 | 57.9 | 2.931 | 0.020 |
| DMD microDYS1 | 27 | 65 | 41.5 | 0.197 | > 0.999 |
| DMD microDYS2 | 23 | 53 | 43.4 | 0.473 | > 0.999 |
| DMD microDYS3 | 24 | 56 | 42.9 | 0.256 | > 0.999 |
| DMD miniDYS | 25 | 58 | 43.1 | 0.304 | > 0.999 |
| **Fig. S13A** DMD16 | **Arrhythmic** | | | | |
| | **Count** | **Total** | **% of Total** | **Adjusted Residual** | **Corrected p-value** |
| Control Empty | 19 | 63 | 30.2 | -0.396 | > 0.999 |
| DMD Empty | 22 | 61 | 36.1 | 0.700 | > 0.999 |
| DMD microDYS1 | 12 | 52 | 23.1 | -1.539 | 0.743 |
| DMD microDYS2 | 18 | 51 | 35.3 | 0.501 | > 0.999 |
| DMD microDYS3 | 26 | 50 | 52.0 | 3.228 | 0.007 |
| DMD miniDYS | 14 | 67 | 20.9 | -2.219 | 0.159 |

**Table S6. DEGs unique to miniDYS and microDYS3 in Figure S14.** The first tab of the spreadsheet contains DEGs unique to DMD miniDYS. To identify genes unique to DMD miniDYS, we compared differentially expressed genes from DMD miniDYS against both Control Empty and DMD Empty as references and excluded genes that were differentially expressed in DMD microDYS1, DMD microDYS2, and DMD microDYS3. The second tab of the spreadsheet contains DEGs unique to DMD microDYS3 in which we compared differentially expressed genes from DMD microDYS3 against both Control Empty and DMD Empty as references and excluded genes that were differentially expressed in DMD microDYS1, DMD microDYS2, and DMD miniDYS. Negative log2 fold change means downregulated in the condition with respect to reference. Positive log2 fold change means upregulated in the condition with respect to reference. DEGs were assessed with Transcript IDs. DEGs were defined with a cutoff value of absolute $\log_2$ fold change >1 and FDR <0.05.

**Table S7. Power Analyses.** The spreadsheet contains results from pairwise comparison power analysis conducted for DMD19, UC, and DMD16. Effect sizes (Cohen's d) and computed power are provided. The first three tabs of the spreadsheet contain results from cell viability power analyses. The next three tabs of the spreadsheet contain results from cell size power analyses. The next three tabs contain results from nuclear size power analyses. The last 12 tabs contain results from RT-qPCR power analyses.

**Table S8. Transfer plasmids for lentivirus production.** Plasmids are listed with their original names, alias, and dystrophin variant.

| Transfer Plasmid | Alias | Dystrophin Variant |
|---|---|---|
| pSIN-TNNT2-zeoR | Empty | N/A |
| pSIN-TNNT2-microDYS1-zeoR | microDYS1 | ΔR2-R15/ΔR18-R22/ΔC |
| pSIN-TNNT2-microDYS2-zeoR | microDYS2 | ΔR3-R19/ΔR20-R21/ΔC |
| pSIN-TNNT2-microDYS3-zeoR | microDYS3 | ΔR4-R23/ΔC |
| pSIN-TNNT2-miniDYS-zeoR | miniDYS | ΔH2-R19 |

**Table S9. RT-qPCR primers.** Primers used for qPCR analysis with their forward and reverse sequences (5' to 3').

| Primer | Forward Sequence | Reverse Sequence |
|---|---|---|
| DMD N-terminus | CCAGCTGGTCTGATGGCCTG | GTGTGGCTGACTGCTGGC |
| DMD H1-R1 | CCTTCACAGCATTTGGAAGCTCC | GCTTGCAATGTGTCCTCAGCAG |
| DMD R16-R17 | GTGCAACGCCTGTGGAAAGG | CTGTCAAATCGCCCTTGTCGG |
| DMD H4 | TTCTGCAGGTGGCCGTCG | CCCAGGGACCCTGGACAG |
| GAPDH | GTGGACCTGACCTGCCGTC | GGAGACCACCTGGTGCTCAG |

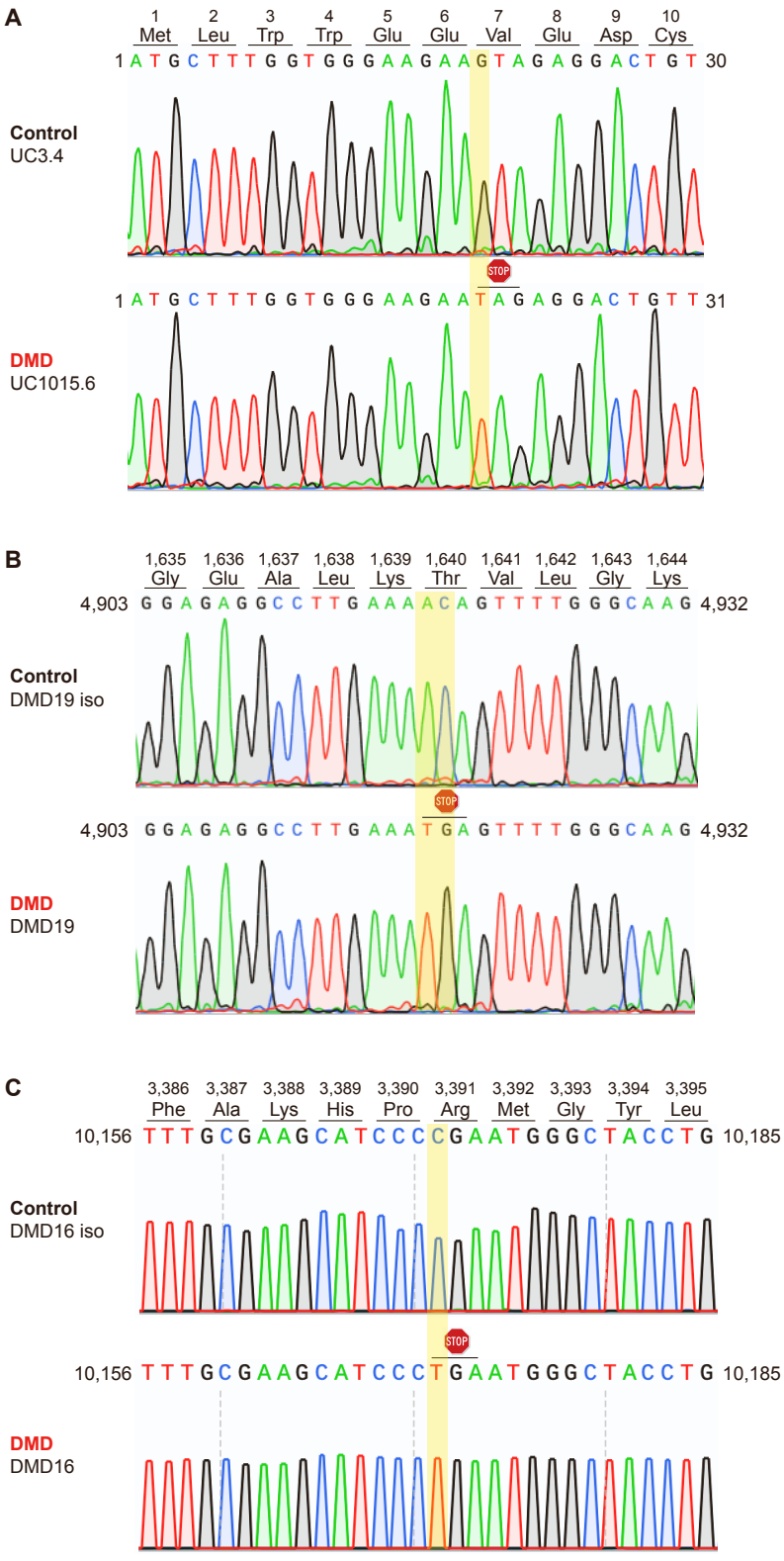


**Figure S1. Sanger sequencing confirms mutational status of iPSC lines.**
Genetic differences between (A) UC3.4 and UC1015.6 (c.19del), (B) DMD19 iso and DMD19 (c.4918_4919AC>TG), and (C) DMD16 iso and DMD16 (c.10171C>T) iPSC lines.

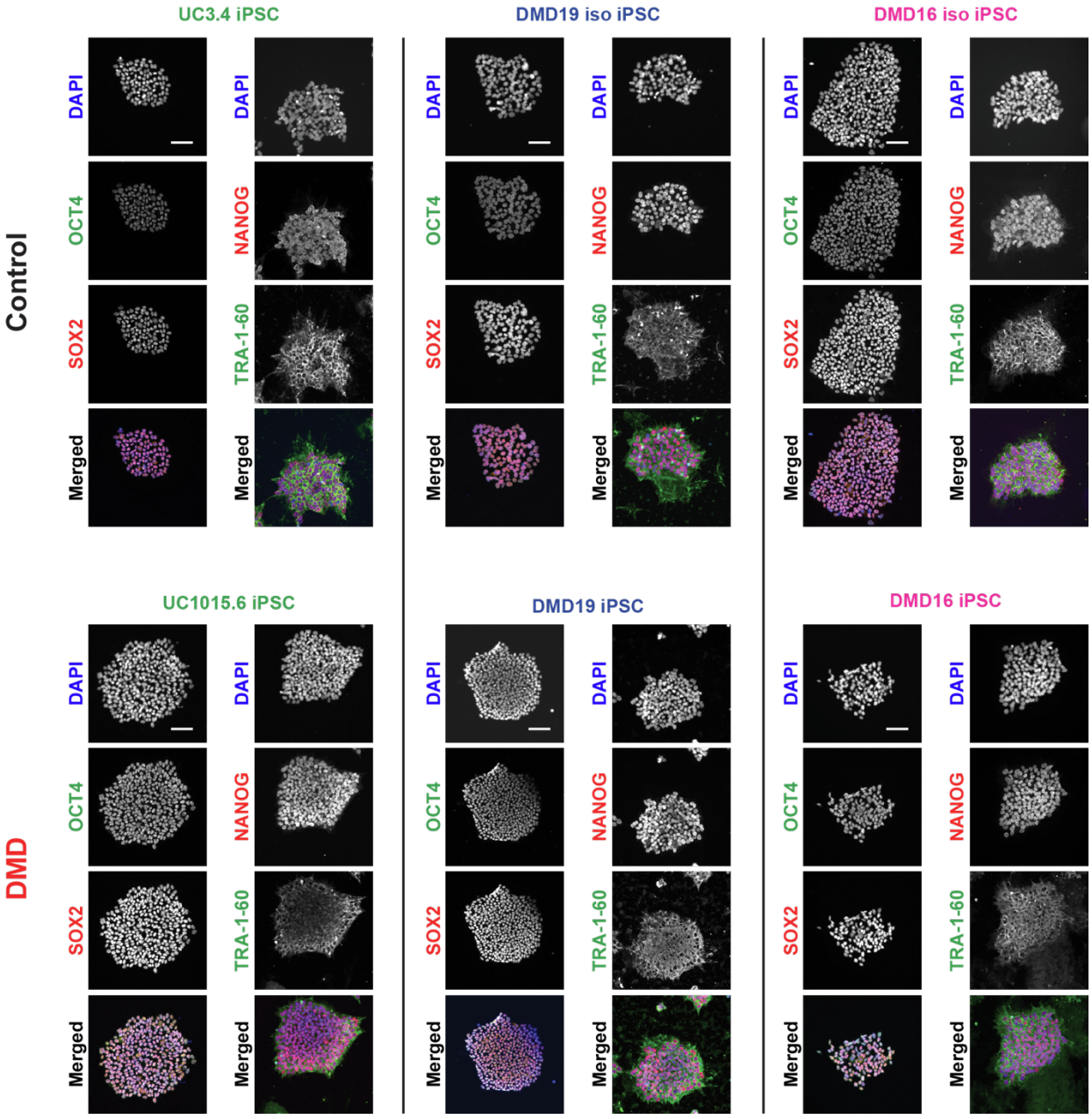


**Figure S2. Markers of pluripotency expressed by iPSCs**.
Immunostaining for OCT4, SOX2, NANOG, and TRA-1-60 for each cell line. Scale bar is 100 μm.

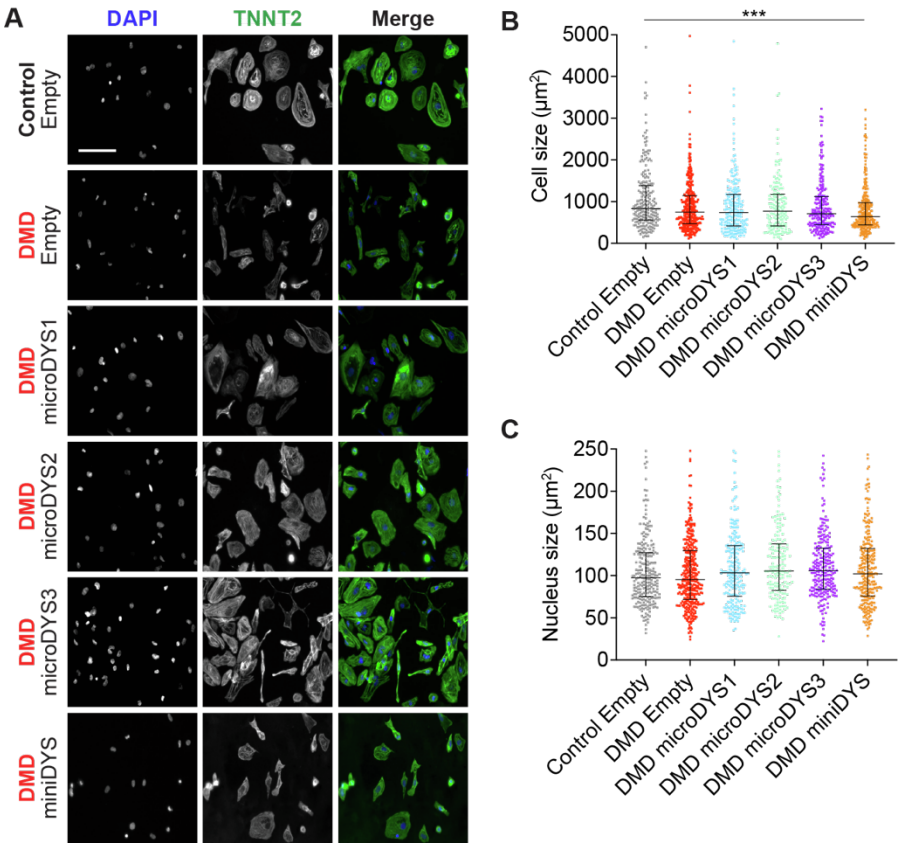


**Figure S3. Differentiation of UC line to iPSC-CMs.**
(A) TNNT2 immunostaining of UC iPSC-CMs. DAPI marks nuclei. Scale bar, 100 μm. (B) Cell size and (C) nucleus size quantification of UC iPSC-CMs. Data represent median with interquartile ranges from at 3-6 experiments. n = 158-354 cells. One-way ANOVA and Kruskal-Wallis test for post-hoc comparison at $p<0.05$. ***$p<0.001$

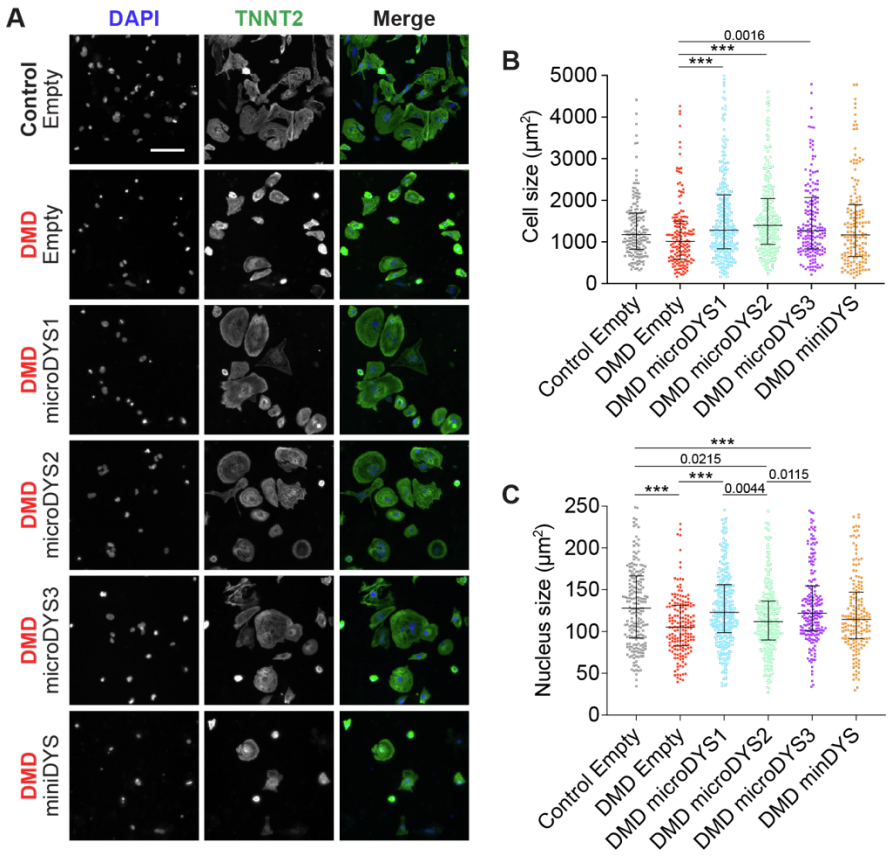


**Figure S4. Microdystrophins restore reduced cell size in DMD16 iPSC-CMs.**
(A) TNNT2 immunostaining of DMD16 iPSC-CMs. DAPI marks nuclei. Scale bar, 100 μm.
(B) Cell size and (C) nucleus size quantification of DMD16 iPSC-CMs. Data represent median with interquartile ranges from 3-5 experiments. n = 157-340 cells. One-way ANOVA and Kruskal-Wallis test for post-hoc comparison. *** $p < 0.001$

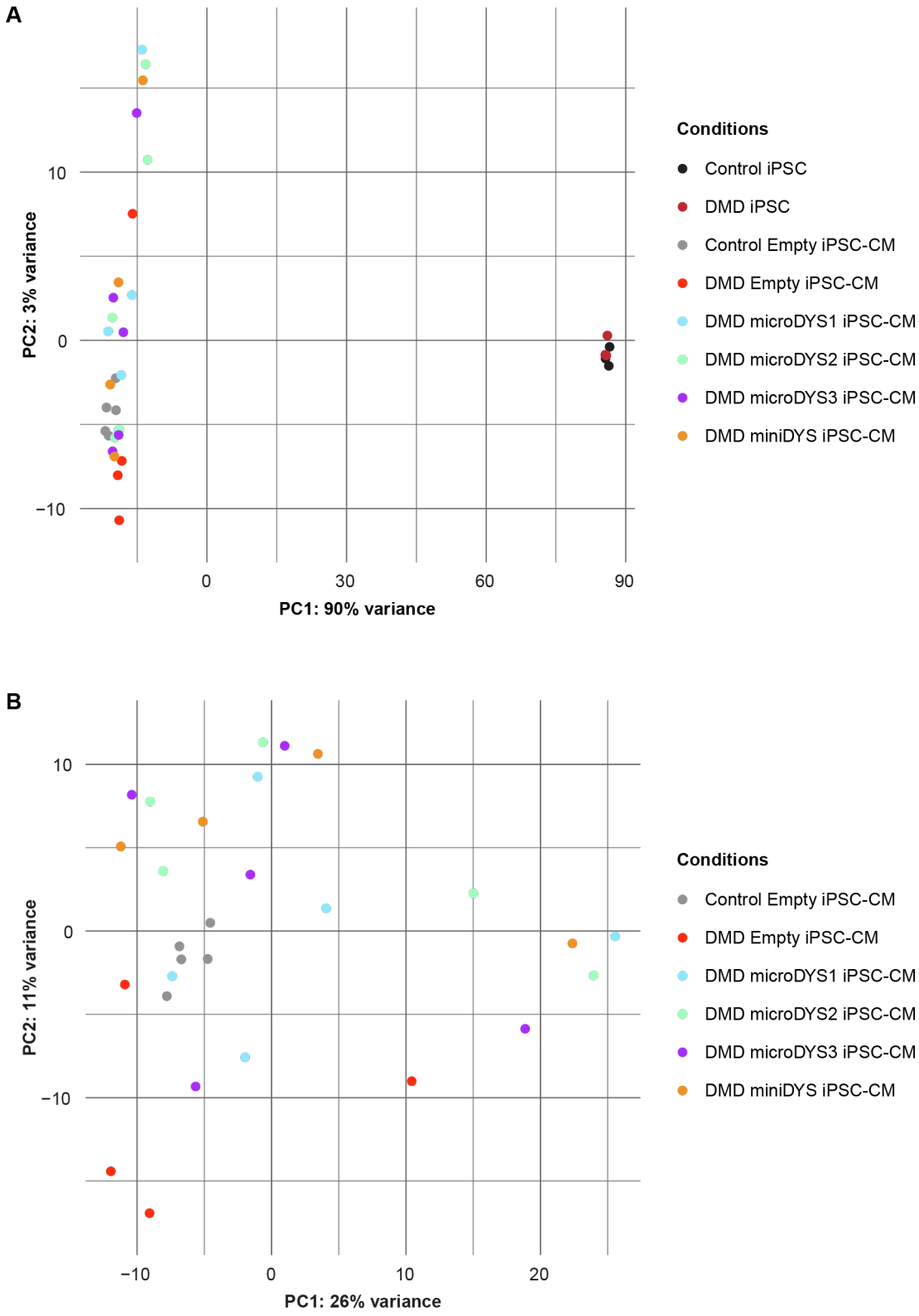


**Figure S5. Principal component analysis of RNA-sequencing data of DMD19.**
(A) Principal component analysis (PCA) of iPSCs and iPSC-CMs. (B) PCA of iPSC-CMs only.

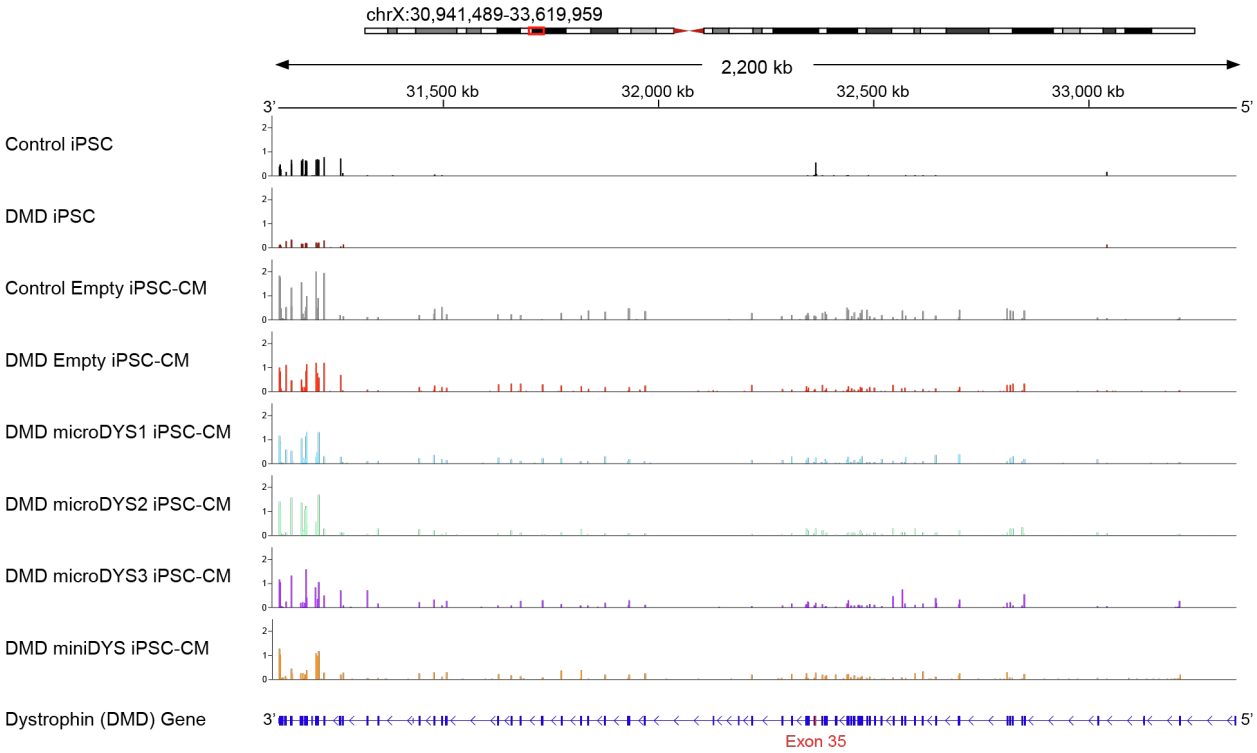


**Figure S6. Visualization of DMD19 Bulk RNA-Sequencing Reads.**
Integrative genomics viewer (IGV) visualization of RNA-Seq alignments at the dystrophin locus. Coverage tracks show pileup of reads across Control iPSC, DMD iPSC, Control Empty iPSC-CM, DMD Empty iPSC-CM, DMD microDYS1 iPSC-CM, DMD microDYS2 iPSC-CM, DMD microDYS3 iPSC-CM, and DMD miniDYS iPSC-CM. The dystrophin reference sequence is in dark blue, with exons represented as rectangles. The gene is displayed in the antisense direction from 3' to 5'. The DMD19 line has a nonsense mutation in exon 35.

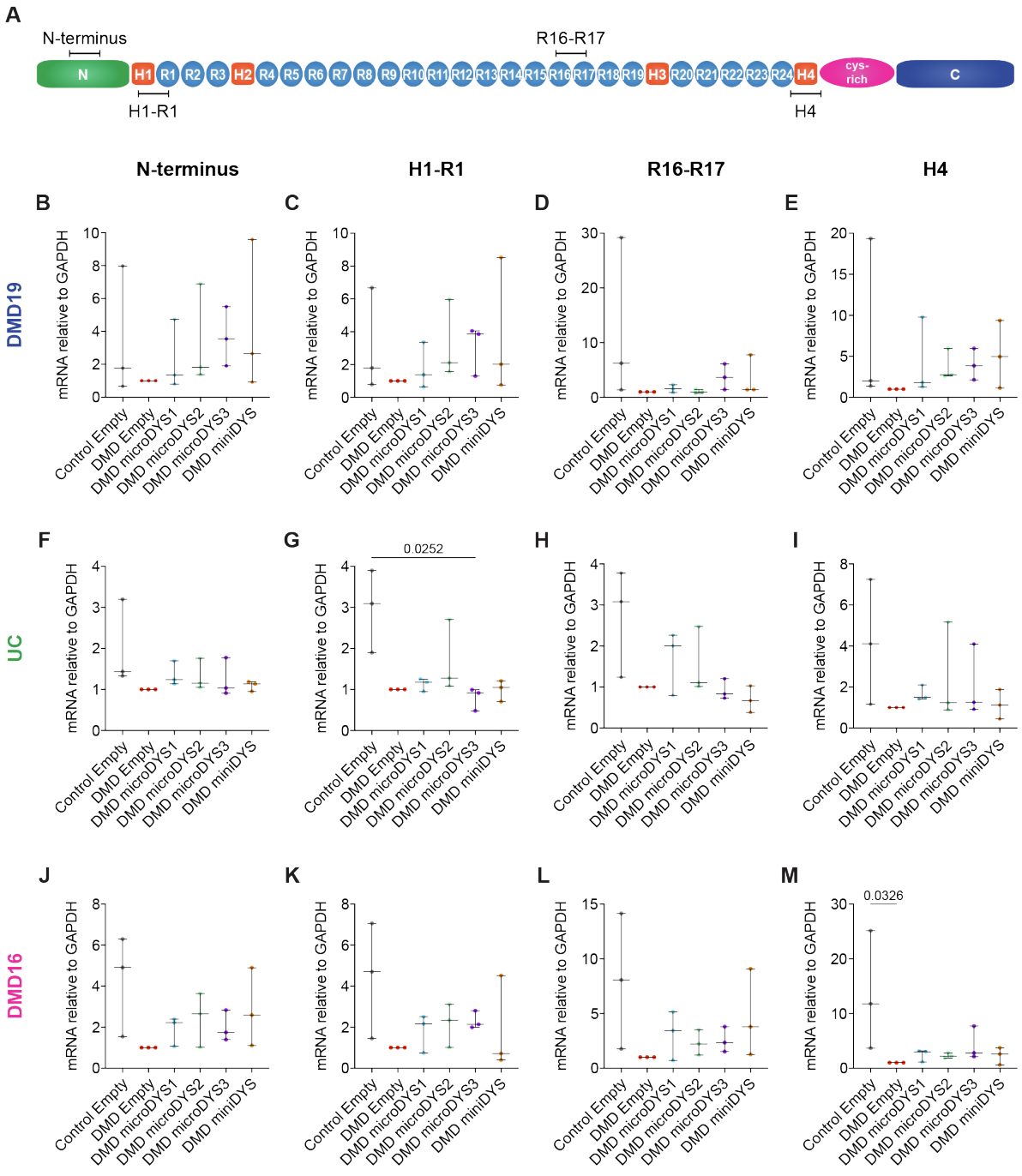


**Figure S7. RT- qPCR quantification of dystrophin mRNA normalized to DMD Empty iPSC-CMs.**

mRNA expression of dystrophin relative to GAPDH in Day 30 iPSC-CMs. (A) Schematic shows domains of dystrophin and amplicons used to quantify mRNA expression along the coding sequence, including the N-terminus, Hinge 1 to Spectrin-like Repeat 1, Spectrin-like Repeats 16-17, and Hinge 4. mRNA expression relative to GAPDH is quantified in the DMD19 line (B, C, D, E), the UC line (F, G, H, I), and DMD16 line (J, K, L, M). Data represent median with interquartile range from 3 differentiation experiments. One-way ANOVA and Kruskal-Wallis test were used to determine significance at $p<0.05$.

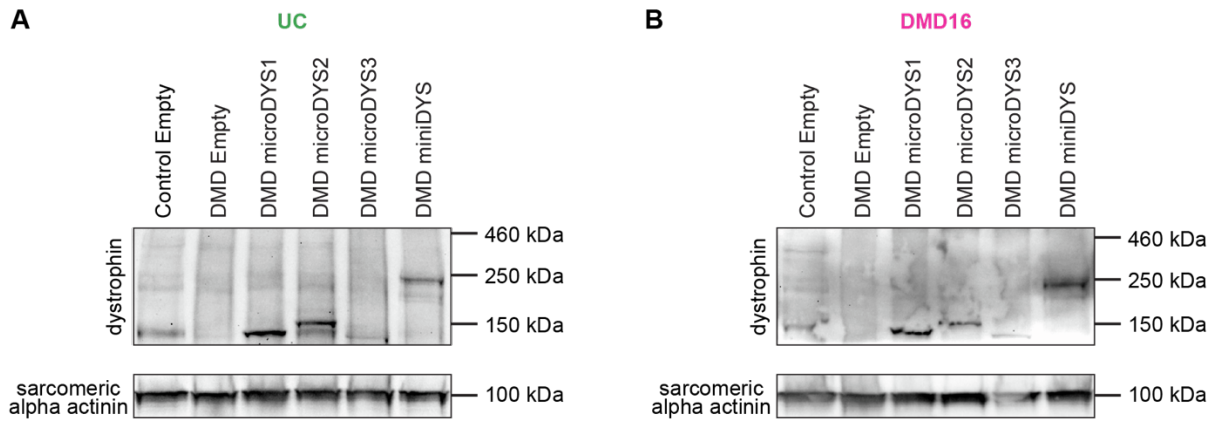


**Figure S8. Transgene expression by western in Day 30 iPSC-CMs.** Western blot of dystrophin levels with sarcomeric alpha actinin as a loading control in (A) the UC line and (B) the DMD16 line. Expected sizes are 427 kDa for full-length dystrophin, 147 kDa for microDYS1, 153 kDa for microDYS2, 138 kDa for microDYS3, 222 kDa for miniDYS, and 104 kDa for sarcomeric alpha actinin.

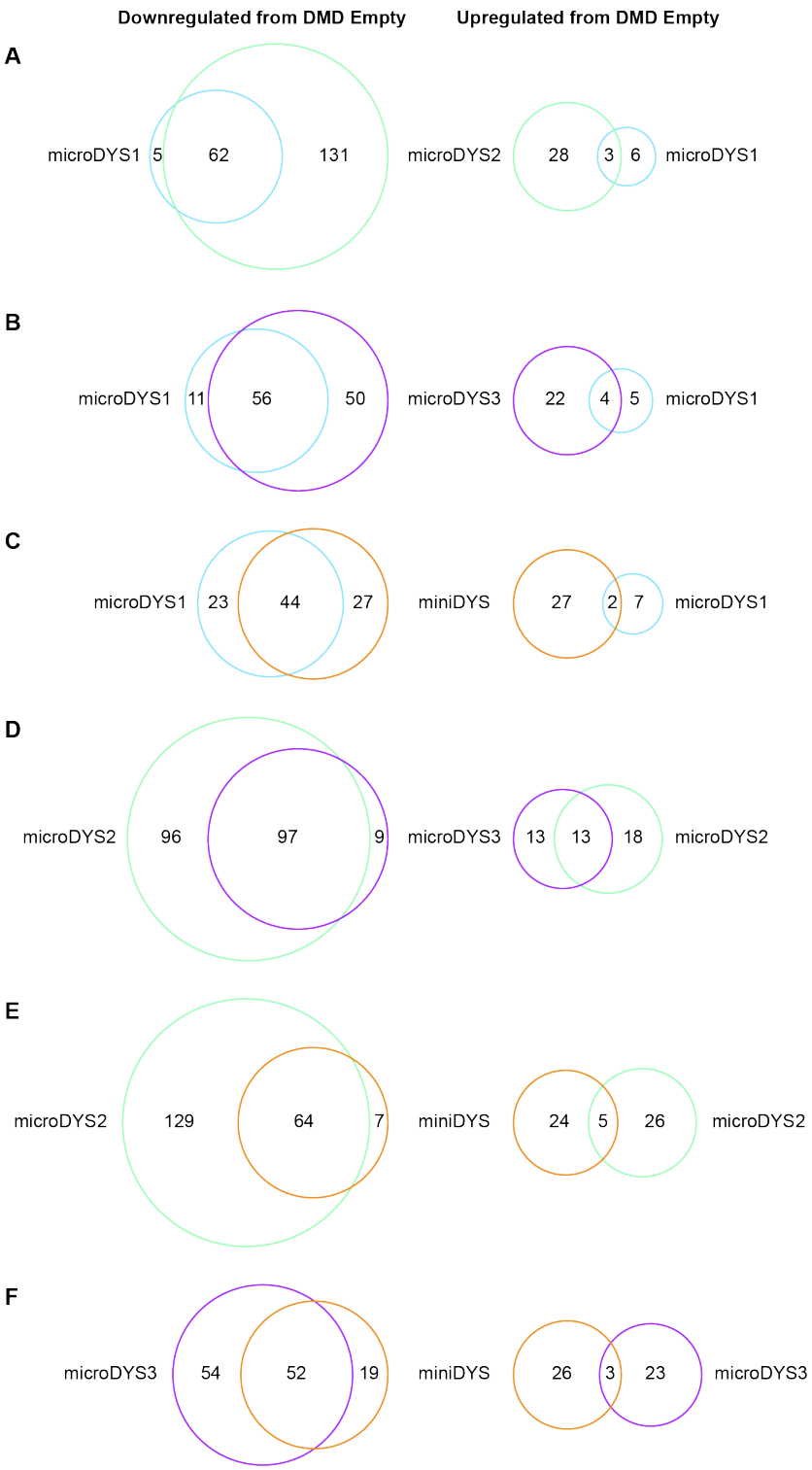


**Figure S9. Shared DEGs among treatments with DMD Empty as a refence in the DMD19 background.**
DEGs for each condition compared to DMD Empty iPSC-CMs. DEGs were defined with a cutoff value of absolute $log_2$ fold change >1 and FDR <0.05. Downregulated ($log_2$ fold change <-1) DEGs on left and upregulated ($log_2$ fold change >1) on the right. Venn diagrams represent shared DEGs between (A) microDYS1 and microDYS2, (B) microDYS1 and microDYS3, (C) microDYS1 and miniDYS, (D) microDYS2 and microDYS3, (E) microDYS2 and miniDYS, and (F) microDYS3 and miniDYS.

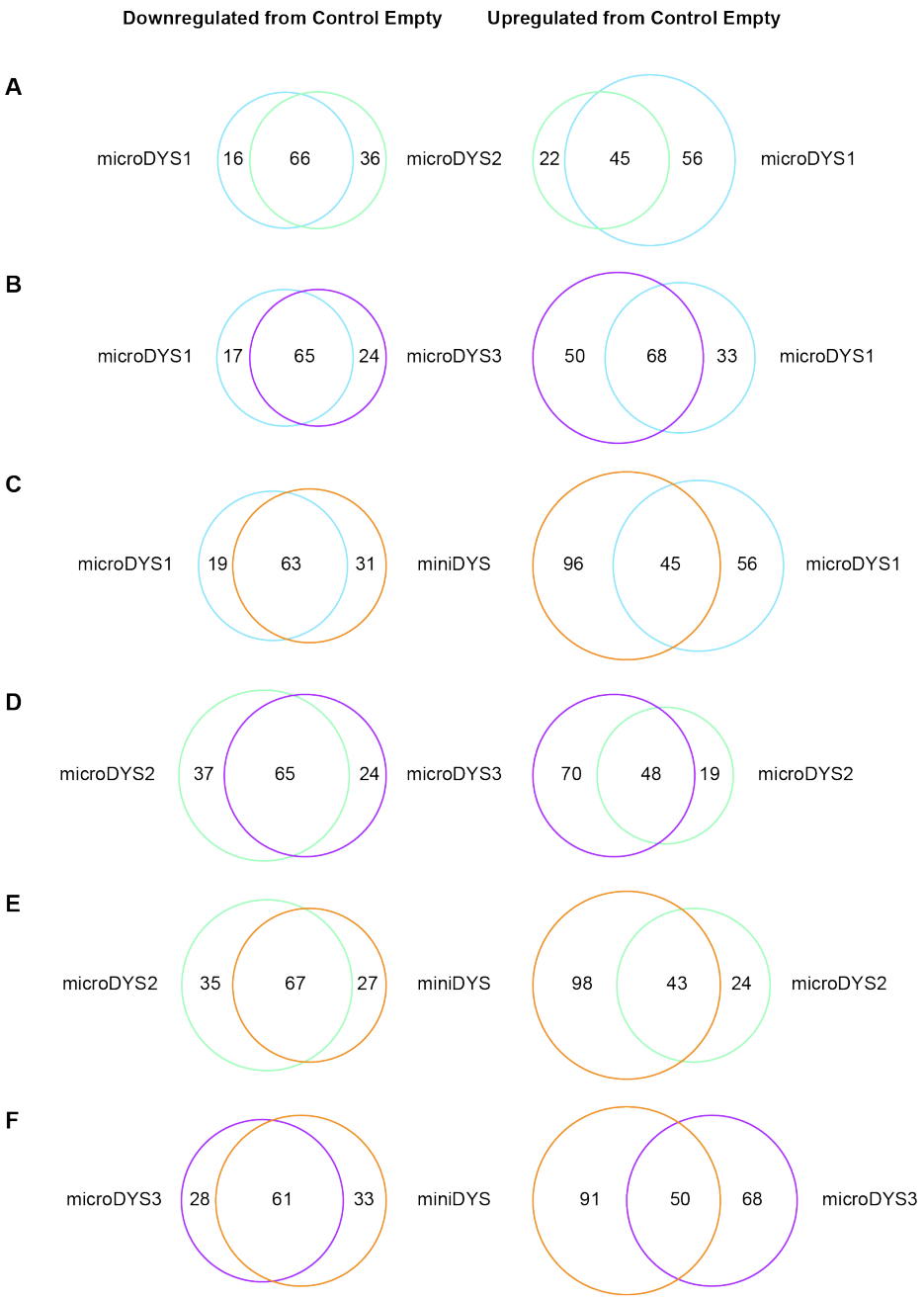


**Figure S10. Shared DEGs among treatments with Control Empty as a reference in the DMD19 background.**
DEGs for each condition compared to Control Empty iPSC-CMs. DEGs were defined with a cutoff value of absolute $\log_2$ fold change >1 and FDR <0.05. Downregulated ($\log_2$ fold change <-1) DEGs on left and upregulated ($\log_2$ fold change >1) on the right. Venn diagrams represent shared DEGs between (A) microDYS1 and microDYS2, (B) microDYS1 and microDYS3, (C) microDYS1 and miniDYS, (D) microDYS2 and microDYS3, (E) microDYS2 and miniDYS, and (F) microDYS3 and miniDYS.

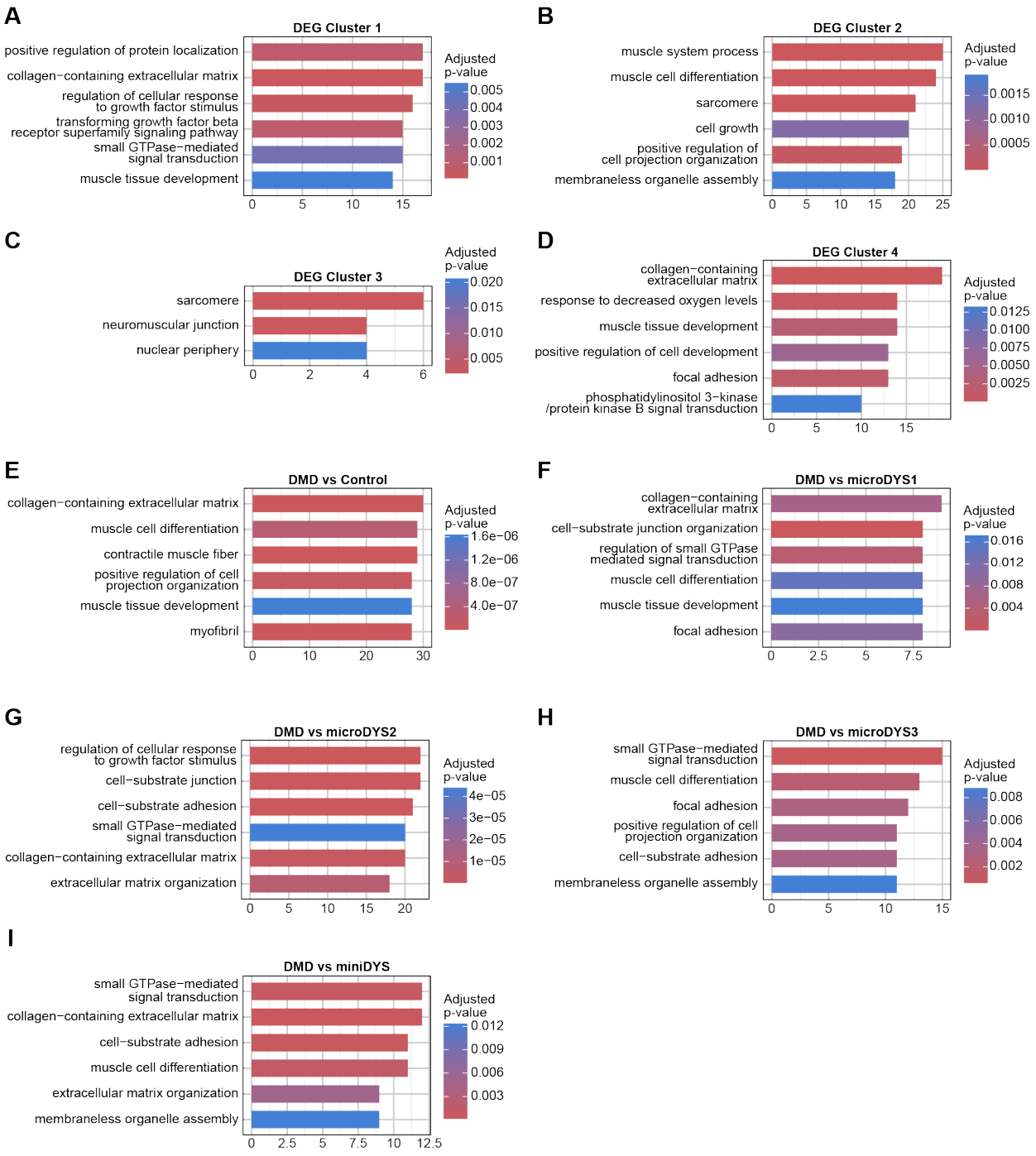


**Figure S11. Gene Ontology enrichment analysis in DMD19.**
Number of DEGs for each Gene Ontology (GO) term indicated on x-axis for each pairwise comparison. DEGs were defined with a cutoff value of absolute $\log_2$ fold change >1 and FDR <0.05. GO terms associated with DEG clusters in Figure 3F: (A) Cluster 1, (B) Cluster 2, (C) Cluster 3, and (D) Cluster 4. (E) DMD Empty vs Control Empty, (F) DMD Empty vs DMD microDYS1, (G) DMD Empty vs DMD microDYS2, (H) DMD Empty vs DMD microDYS3, (I) DMD Empty vs DMD miniDYS.

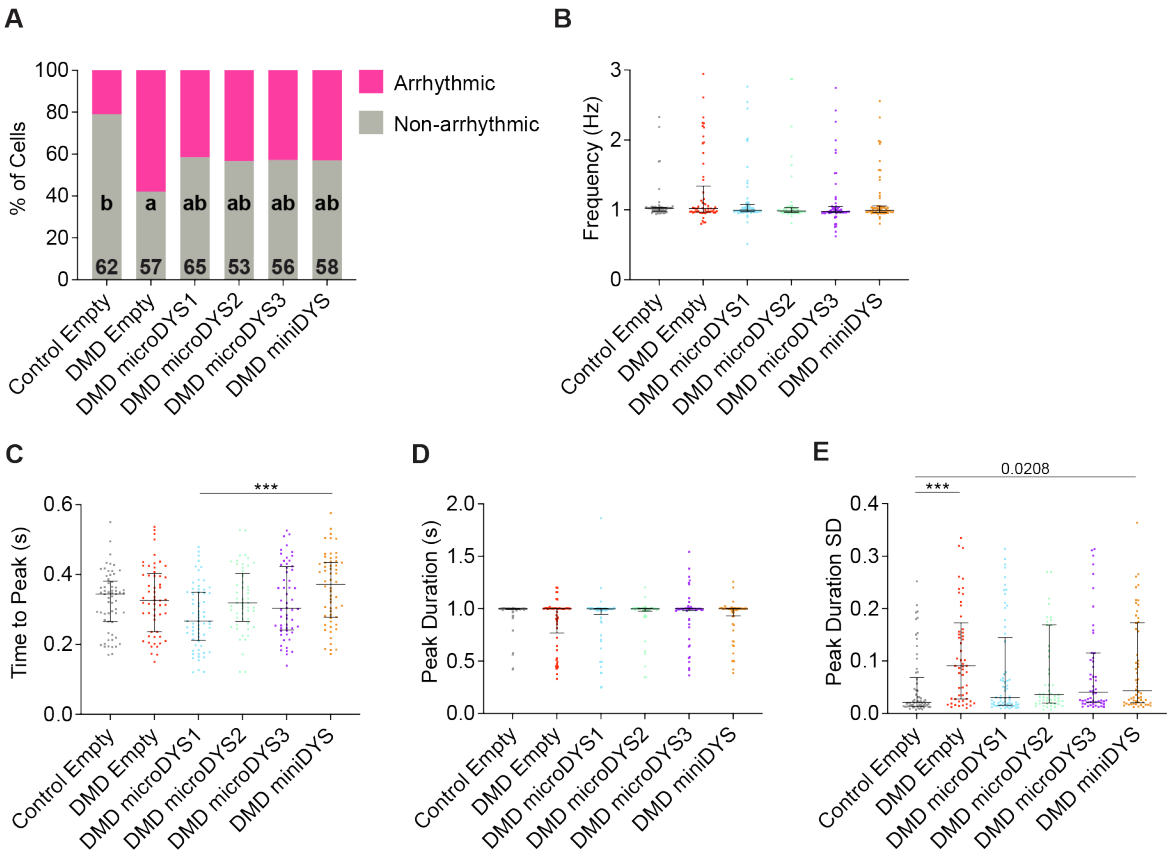


**Figure S12. Calcium handling in the UC background.**
(A) Frequency of arrhythmia in UC iPSC-CMs. The percentage of cells is defined as the number of cells in a given category divided by the total number of cells. A chi-square test was used to determine significance. Different letters indicate statistical significance at $p<0.05$. (B) Frequency, (C) time to peak, (D) peak duration, and (E) standard deviation of peak duration in UC iPSC-CMs. Data represent median with interquartile ranges from 4-6 differentiation experiments with 53-62 cells per condition. One-way ANOVA and Kruskal-Wallis test for post-hoc comparison at $p<0.05$. ***$p<0.001$.

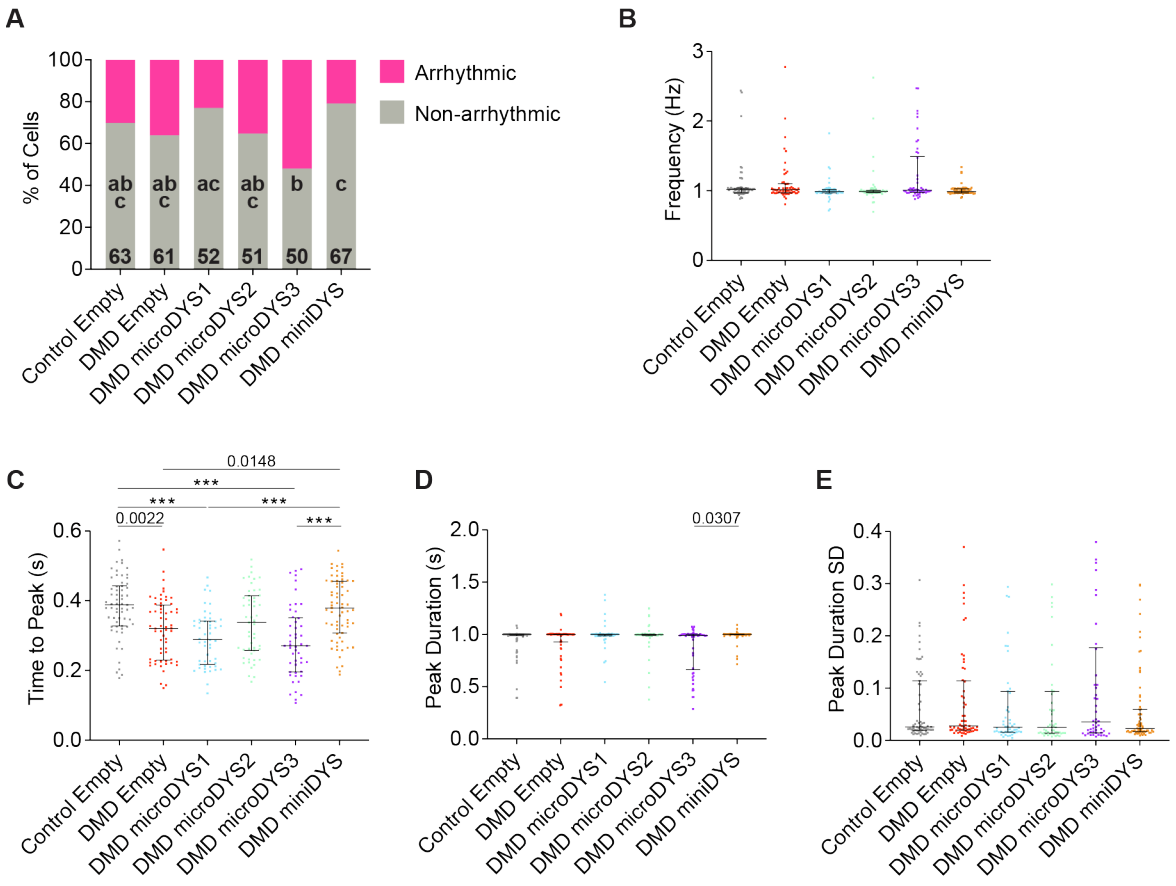


**Figure S13. Calcium handling in the DMD16 background.**
(A) Frequency of arrhythmia in DMD16 iPSC-CMs. The percentage of cells is defined as the number of cells in a given category divided by the total number of cells. A chi-square test was used to determine significance. Different letters indicate statistical significance at $p < 0.05$. (B) Frequency, (C) time to peak, (D) peak duration, (E) and standard deviation of peak duration for DMD16 iPSC-CMs. Data represent median with interquartile ranges from 5-6 differentiation experiments with 50-67 cells per condition. One-way ANOVA and Kruskal-Wallis test for post-hoc comparison at $p<0.05$. ***$p<0.001$.

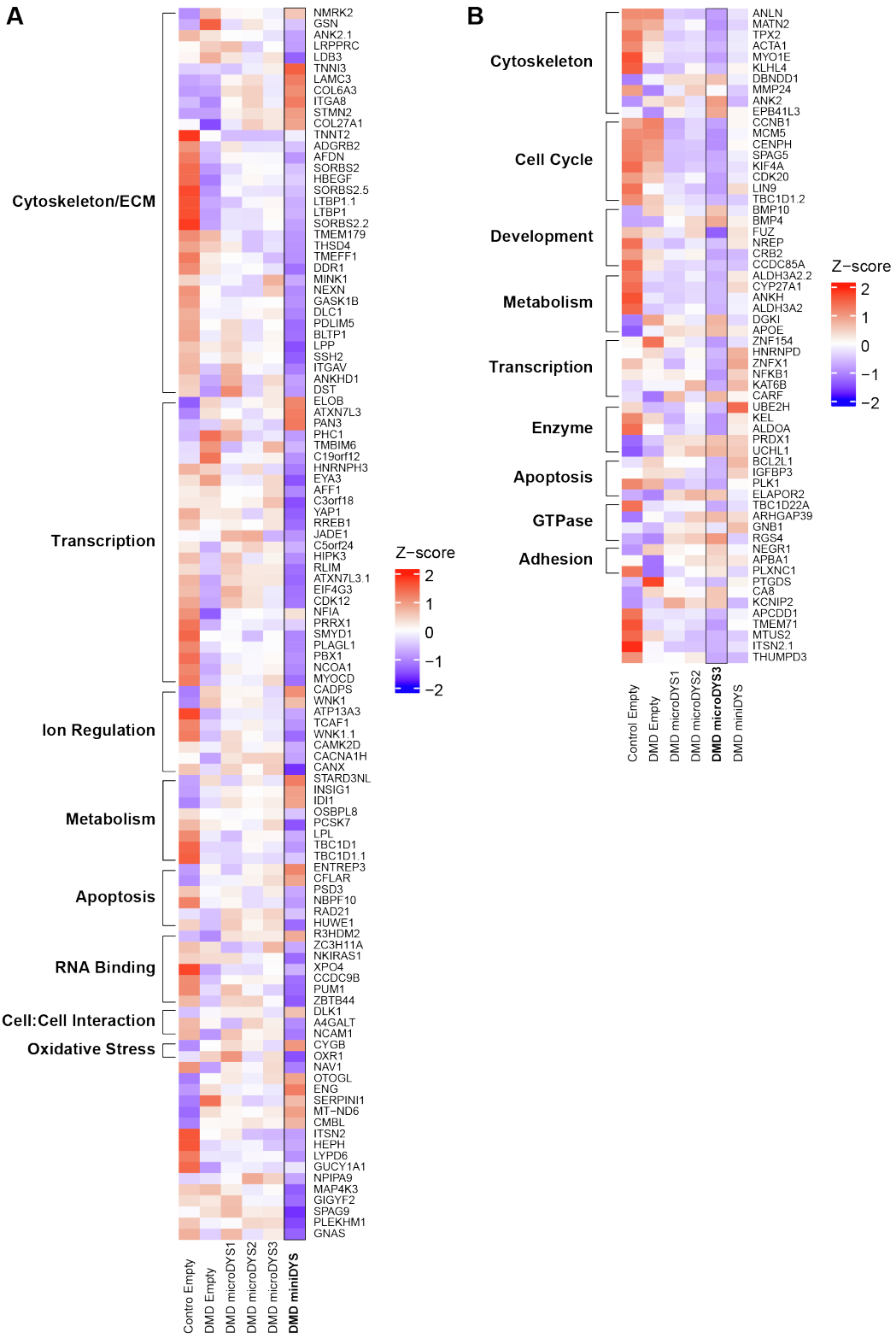


**Figure S14. Genes related to cytoskeleton and transcription rescue disease phenotypes in DMD iPSC-CMs.** Heatmap of differentially expressed genes (DEGs) unique to (A) DMD miniDYS iPSC-CMs and (B) DMD microDYS3 iPSC-CMs. Genes unique to DMD miniDYS were identified by comparing DMD miniDYS to both reference conditions (Control Empty and DMD Empty) and retaining only genes that were differentially expressed in DMD miniDYS but not shared with any of the other three treatment groups (DMD microDYS1, DMD microDYS2, and DMD microDYS3). Genes unique to DMD microDYS3 were identified in the same manner by

comparing DMD microDYS3 to both reference conditions (Control Empty and DMD Empty) and retaining only genes that were differentially expressed in DMD microDYS3 but not shared with any of the other three treatment groups (DMD microDYS1, DMD microDYS2, and DMD miniDYS).

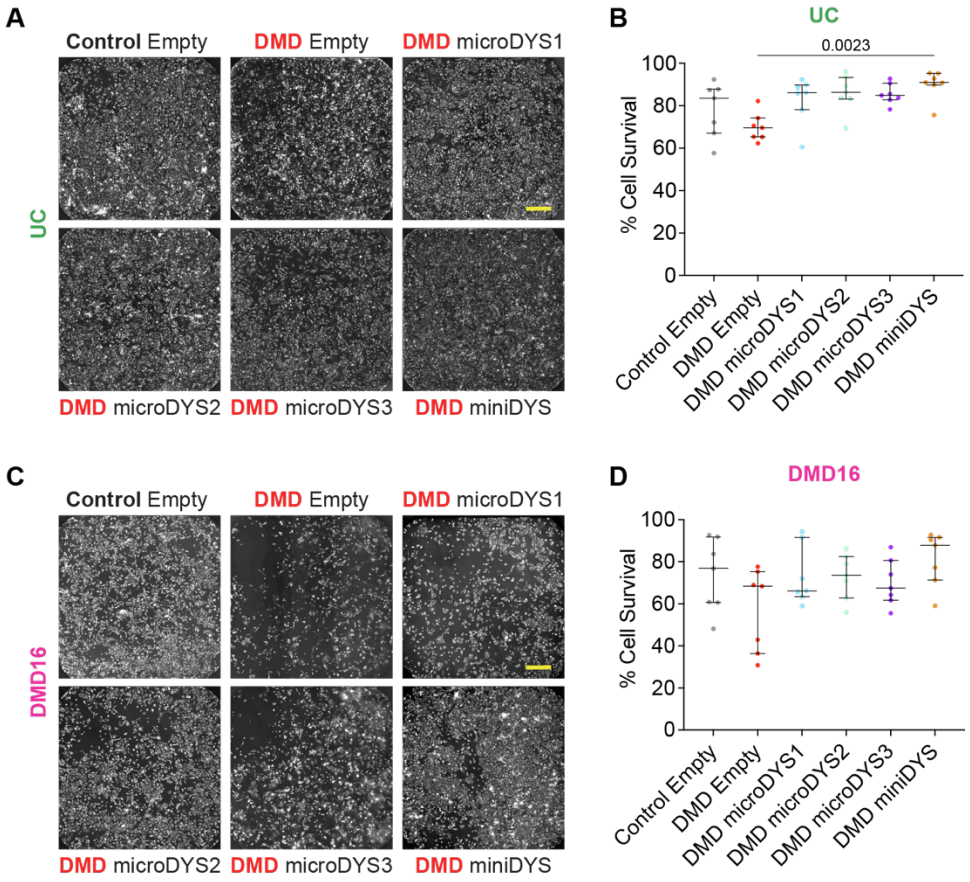


**Figure S15. Cell viability assays in the UC and DMD16 background.**
(A) Representative wells stitched from 12 images of UC iPSC-CMs loaded with TMRM on Day 38. Scale bar = 500 μm. (B) Quantification of cell survival for UC iPSC-CMs. Data represent median with interquartile range from 7 differentiation experiments. One-way ANOVA and Kruskal-Wallis test for post-hoc comparison. (C) Representative wells stitched from 12 images of DMD16 iPSC-CMs loaded with TMRM on Day 38. Scale bar, 500 μm. (D) Quantification of cell survival for DMD16 iPSC-CMs. Data represent median with interquartile ranges from 7 differentiation experiments. One-way ANOVA and Kruskal-Wallis test for post-hoc comparison at $p<0.05$. No pairwise comparison was statistically significant.

**Video S1.** Spontaneously contracting Day 30 iPSC-cardiomyocytes in the DMD19 background. DMD19 cardiomyocytes beating on Day 30 of differentiation for Control Empty, DMD Empty, DMD microDYS1, DMD microDYS2, DMD microDYS3, and DMD miniDYS. Scale bar, 100 μm.

**Video S2.** Spontaneously contracting Day 30 iPSC-cardiomyocytes in the UC background. UC cardiomyocytes beating on Day 30 of differentiation for Control Empty, DMD Empty, DMD microDYS1, DMD microDYS2, DMD microDYS3, and DMD miniDYS. Scale bar, 100 μm.

**Video S3.** Spontaneously contracting Day 30 iPSC-cardiomyocytes in the DMD16 background. DMD16 cardiomyocytes beating on Day 30 of differentiation for Control Empty, DMD Empty, DMD microDYS1, DMD microDYS2, DMD microDYS3, and DMD miniDYS. Scale bar, 100 μm.